Version of Record: https://www.sciencedirect.com/science/article/pii/S0022407318307374
Manuscript_a08a193218712b2b20b79bd0f45f939a

A multi-wavelength speciation framework for high-temperature hydrocarbon pyrolysis

Nicolas H. Pinkowski*, Yiming Ding, Sarah E. Johnson, Yu Wang, Thomas C. Parise, David F. Davidson, Ronald K. Hanson

High Temperature Gasdynamics Laboratory, Department of Mechanical Engineering, Stanford University, Stanford, CA 94305-3032, USA

Abstract

A framework for the study of high-temperature hydrocarbon pyrolysis is presented. The proposed framework details a multi-wavelength speciation method using convex optimization, a review of complementary fixed-wavelength laser diagnostics, and a database of high-temperature absorption cross-sections to enable use of the framework for 11 different species. The proposed speciation method involves a vectorized Beer-Lambert system solved under solution constraints using convex optimization. In support of the proposed method, a review of pertinent laser diagnostics and a database of high-temperature absorption cross-sections are also provided. The database includes measured absorption cross-sections of methane (CH_4), ethylene (C_2H_4), propene (C_3H_6), iso-butene (i-C_4H_8), 1-butene (1-C_4H_8), benzene (C_6H_6), toluene (C_7H_8), and four jet fuels (samples of Jet A, JP5, JP8, and Gevo ATJ) at the wavelengths of 3.1758 µm, 3.17595 µm, 3.283 µm, 3.392 µm, 3.410 µm, 10.532 µm, 10.675 µm, 10.89 µm, 10.958 µm, 10.962 µm, and 11.345 µm within the range of 300-1600 K and 0.25-4 atm. The database is comprised of over 1000 high–temperature absorption cross-section measurements from new shock tube experiments, new Fourier transform infrared spectrometer (FTIR) experiments, and an aggregated dataset from the literature. The convex speciation method and cross-section database provided will facilitate laser absorption studies of hydrocarbon pyrolysis used in the development of chemical kinetic mechanisms.

Keywords: cross-section, mid-infrared, absorption spectroscopy, hydrocarbon pyrolysis, high-temperature, shock tube, methane, ethylene, propene, butene, toluene, benzene, jet fuel, convex optimization

1. Introduction

In many studies of real fuel performance with laser absorption spectroscopy, scientists and engineers do not measure the spectrum of a single species, but rather a composite spectrum of a blend of species which must be interpreted. Determination of the underlying chemical makeup that creates the composite spectrum is amenable when the infrared spectra of all constituent species are known and the spectrum of the mixture can readily be measured. When only portions of the spectra can be measured, and limited knowledge of the spectra is available, interpretation of the composition spectra becomes much more complex. In recent years, there has been interest to measure the instantaneous composition of high-temperature, fast-reacting systems [1-5]. Such speciation is readily achieved at lower temperatures, where lower time-resolution is required, and a number of spectroscopic databases exist for such temperature ranges [6-9]. The same cannot be said for high-temperature environments where there is limited cross-section information and the temporal resolution requirements limit measurement techniques that can be used.

The authors' motivation for characterizing high-temperature, rapidly-changing gaseous environments is in support of chemical kinetics studies of alternative jet fuels. With the emergence of drop-in fuels and ambitious plans to adopt and deploy such fuels [1-2], there is a need to accelerate the timeline and decrease the costs associated with new fuel certification. Kinetic study of fuel pyrolysis at temperatures above 1000 K is a recent focus of alternative fuel investigations [10-12]. For such reactive chemistry, speciation measurements require high time-resolution in order to provide the information needed for kinetic model validation and for the construction of the recently developed hybrid chemistry kinetic models [12-15]. Achieving speciation measurements with high time-resolution presents a great challenge that excludes methods such as gas chromatography (GC), Fourier transform infrared spectrometers (FTIR), and mass spectrometers that are used with flow reactors, static cells, or single pulse shock tubes. Among high-bandwidth measurement techniques, laser absorption spectroscopy is well positioned to characterize fuel chemistry and be utilized in conjunction with pressure driven shock tubes.

Assuming the high-temperature spectra of all key species are known *a priori*, time-resolved composition of fast reacting systems can be determined by probing the underlying blended spectrum at discrete wavelengths and determining what combination of species would best represent the measured spectrum at those wavelengths.

Supposing there is no interfering absorbance from other species, a single wavelength can be used with very high time-resolution to study an individual species during combustion and pyrolysis experiments. Single-wavelength diagnostics have been used in studies of many hydrocarbons including ethylene [16-18], iso-butene [19], and dozens of hydrocarbons at well-documented wavelengths since the 1970's [20-27]. For example, the 3.392μm helium-neon gas laser has been used extensively to study hydrocarbons for many decades [20-27]. However, for blends of absorbing species, more wavelengths of light must be used because the assumption of negligible interfering absorbance must be relaxed. A progression from the single-wavelength method involves the implementation of multiple wavelengths to infer the mole fraction of a species. A two-wavelength "online/offline" method has been used recently to measure methane [28], ethylene [29], and propene [30]. It is important to note that online/offline diagnostics require an assumption of wavelength-independent absorption by all interfering species between the two wavelengths selected. While such an assumption can be appropriate for small molecules with discrete spectra and wavelengths that are spectrally close, in a blended spectrum this assumption can lead to systematic error if the online/offline wavelengths are a significant distance apart and the features studied are broad.

An alternative to the online/offline approach involves the use of multiple wavelengths and solving for several species simultaneously using a matrix method. For a simple mixture of only two species, two wavelengths can be used simultaneously to measure both species. A two-species, two-wavelength matrix method approach was most recently employed by Parise et al. [31] to measure both ethylene and propene during propene pyrolysis. Although small matrix methods have been employed previously [11,31], a multi-species, multi-wavelength framework is yet to be formalized and extended past small systems. Furthermore, *a priori* knowledge of the high-temperature spectra required for larger matrix methods for hydrocarbon fuel pyrolysis does not yet exist.

The present study seeks to advance a matrix method approach to facilitate the study of high-temperature systems of CH_4, C_2H_4, C_3H_6, i-C_4H_8, 1-C_4H_8, C_6H_6, C_7H_8, and common jet fuels. Accordingly, the current study will (1) propose a mathematical framework that is well-suited for multi-wavelength, multi-species measurements, (2) review existing species diagnostics and suggest a new wavelength for benzene and toluene, and (3) present a database of high-temperature absorption cross-sections to enable future multi-wavelength speciation studies. Measurements from new experiments, in conjunction with data from the literature, are provided for 11 species at 11 wavelengths. The absorption cross-sections provided are within the range of 300-1600K and 0.25-4 atm with the conditions reported for each correlation. Although developed for the primary application of advancing the study of jet fuel chemical kinetics, knowledge of the high-temperature absorption spectra of gaseous molecules enables other applications where the composition of a high-temperature system is desired.

2. Background

2.1. Laser absorption spectroscopy

The high temporal resolution afforded by laser absorption spectroscopy is derived largely from the use of narrow-linewidth continuous-wave (CW) laser sources. Laser absorption diagnostics measure the attenuation of light in an absorbing medium and use the Beer-Lambert relation of Eq. 1 for determination of physical properties of the medium. The absorbance of a gas sample (α) is determined by measuring the ratio of the unattenuated laser intensity (I_0) and attenuated intensity (I) of light passing through a gas sample. Absorbance in the current study is defined as the negative natural logarithm of I/I_0. The measured laser absorbance is proportional to the number density of the absorbing gas sample (n) and optical path length (L). The coefficient, , is a proportionality factor that relates the measured absorbance (α) to the number density and path length.

$$\alpha = -\ln\left(\frac{I}{I_0}\right) = n \quad L \tag{1}$$

Knowledge of the proportionality constant , referred to as the absorption cross-section in units of m^2mol^{-1}, enables measurement of the number density of an individual species by using the Beer-Lambert relation. It has been found that the absorption cross-section of a species is functionalized by temperature, pressure, and composition of the gas mixture [21-22]. Often the pressure and bath gas dependency can be neglected for large molecules at high temperatures [22]. Occasionally pressure dependence cannot be neglected, as is the case for small molecules such as methane. In these cases, a bivariate cross-section correlation is required to account for temperature- and pressure-dependence. Bath gas dependency presents itself at low pressures, temperatures, and with small molecules. Within the range of the current study, no bath gas dependency was considered due to the temperature range studied and the molecule size of the species considered. Although methane is included in the current dataset and considered to be a small molecule, methane's absorption cross-section does not show a significant composition dependency in the temperature and pressure regime studied [21-22].

2.2. Absorption spectra

A molecule's absorption spectrum provides, in essence, a fingerprint that can distinguish one species from another. Fig. 1 illustrates an example spectrum for one species, iso-butene (i-C_4H_8), at 323K using spectral data from Pacific Northwest National Laboratory (PNNL) [6]. Highlighted in Fig. 1 are a unique set of molecular vibrations that identify iso-butene and give rise to its characteristic mid-infrared spectrum [32]. The spectrum of iso-butene indicates three potential regions of interest for species sensing: (1) the 3-4 µm region dominated by C-H stretch modes, (2) the 5.5-8µm region dominated by C=C stretch, C-C stretch, and CH_3 deformation modes, and (3) the 10-12 µm region dominated by an in-plane $=CH_2$ bending mode [32]. Iso-butene presents a representative case for the other small alkenes included in the high-temperature database (C_2H_4, C_3H_6, 1-C_4H_8). The 5.5-8 µm region is generally not used due to relatively low absorbance, potentially strong interference from water, and the high cost of lasers and optics that operate in that region.

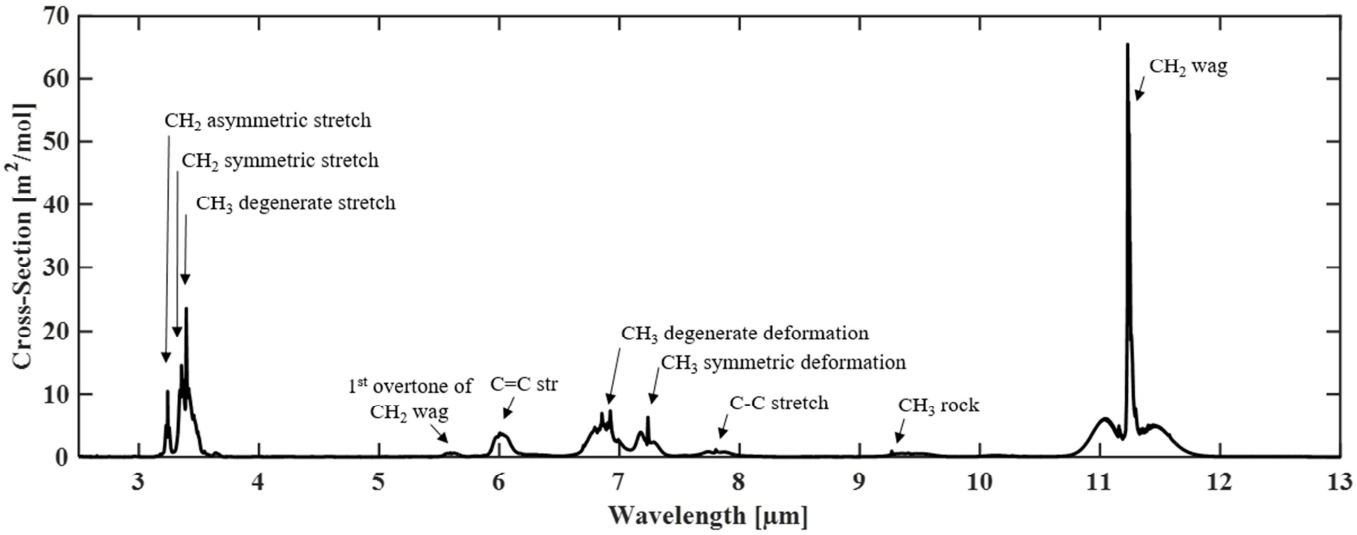

Fig 1: An example absorption spectrum of iso-butene at 323 K and 1 atm available from an FTIR based spectral database [6]. Ten prominent ro-vibrational bands, including two degenerate modes, are shown for the infrared spectrum [32].

When possible, infrared spectra are calculated with theoretical models or measured using FTIR spectrometers. Examples of spectral databases include: PNNL Northwest Infrared, GEISA, NIST, and HITRAN [6-9]. Despite the large number of databases, there is a noted lack of high-temperature spectra for the species of interest. When molecules are small, high-resolution measurements of individual transitions (e.g. see the paper by Cassady et al. [33] for C_2H_2) enable accurate modeling of high-temperature absorption spectra. However, for larger fuels with broadened spectra, determination of each individual transition is not possible. In addition, databases built from FTIR data are typically limited to low temperatures where molecules are thermally stable. Databases built from directly-calculated spectra only exist for a limited number of molecules and temperatures.

Due to the limitations of FTIR and computationally-founded databases, there is an interest in new methods to measure the high-temperature spectra of gaseous molecules. Promising approaches include: (1) the recent work of Strand et al. [34] that employed a new rapid-tuning, broad-scan, External-Cavity Quantum Cascade Laser (EC-QCL), (2) the use of quantum cascade laser frequency combs as reviewed in the work of [35], or (3) selectively probing the high-temperature spectra at discrete wavelengths. The present study focuses on the third approach of probing high-temperature spectra at discrete wavelengths using shock tubes and laser absorption spectroscopy.

2.3. Shock tubes

The proposed speciation framework and supporting absorption cross-sections were developed for, although not limited to, studying chemistry at the high-temperature and -pressure conditions behind reflected shock waves. In this work, two pressure-driven, stainless steel shock tubes with similar dimensions were used to measure all new absorption cross-sections. Each shock tube consisted of 2.8/3.35 meter-long driver gas regions, 9.5/8.54 meter-long driven gas regions, inner diameters of 13.97/14.13 cm, and measurement planes located 1/2 cm from each endwall, respectively. The driven section of the second shock tube was fitted with a jacketed heater and maintained at 353-383 K to increase the vapor pressure of the jet fuels studied. The heated shock tube was coupled with a mixing tank and gas deliver manifold that were also heated, and described in detail in supporting literature [11,14]. Polycarbonate, Lexan, diaphragms separated the driver section from the test section of each shock tube. Steel cross-blade fixtures were used to rupture each diaphragm when a pressure differential of 1 to 3 atm was applied. A shock calculator developed by Campbell et al. [36] enabled accurate determination of the reflected shock conditions using the initial temperature, pressure, and composition of the test gas and a measurement of the incident shock velocity. Shock velocity was measured from five pressure transducers located along the driven section of the shock tube. The shock calculator solves the shock jump equations assuming frozen chemistry and a vibrationally relaxed system. Agreement between the measured and calculated pressure of the reflected shock region supports both assumptions [37].

For a general representation, Fig. 2 (a) depicts the endwall of a shock tube and the passage of a reflected shock wave. Fig. 2(b) presents data from a shock tube experiment with a test gas of 5% 1-butene/Ar heated to 1220 K and 1.73 atm. Three zones are visible in Fig. 2(b): (1) an initial region of low-pressure and -temperature, (2) a second region after the passage of the incident shock wave at an intermediate-pressure and -temperature, and (3) a final region after the passage of the reflected shock wave at a high-pressure (1.73 atm) and -temperature (1220 K). Two representative absorbance time-histories at 3.283 µm and 10.532 µm are shown in Fig 2(b). The absorbance at 10.532 µm is often used to probe the of the out-of-plane bending mode of ethylene, however, is also associated with the in-plane $=CH_2$ bending mode of alkenes such as propene, 1-butene, and 1,3-butadiene. The wavelength of 3.283 µm, shown in black in Fig. 2(b), is a new spectroscopic line developed in the present study. Absorbance at 3.283 µm targets phenylated C-H stretch modes from aromatic molecules but also measures absorbance contributions from the symmetric and asymmetric CH_2 stretch modes of alkanes and alkenes. As ethylene forms, the absorbance at 10.532 µm is seen to increase; as evident from the red time-history in Fig. 2(b). The black absorbance time-history at 3.283 µm is balanced due to increasing absorbance from formation of products countered by decreasing absorbance from 1-butene decomposition.

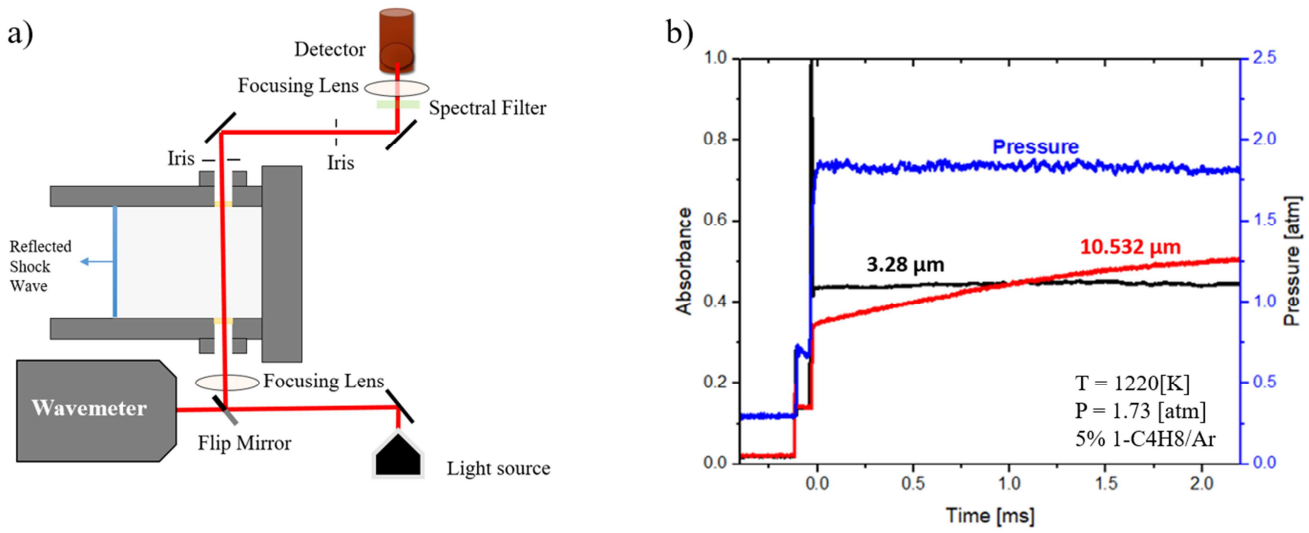

Fig. 2: (a) A detailed schematic of a laser absorption diagnostic located at the endwall of a shock tube showing the passage of a reflected shock. (b) Sample data for a measurement of 5% 1-C_4H_8 in argon at 1220 K, and 1.73 atm. Blue: the pressure time-history measured with a sidewall pressure transducer. Red: the absorbance at 10.532µm with sensitivity to the out-of-plane bending mode of ethylene with contributions from the in-plane =CH_2 bending mode of alkenes. Black: absorbance at 3.283 µm with sensitivity to phenyl groups and with absorbance contributions from CH_2 symmetric and asymmetric stretch modes.

2.4. Lasers and Optics

Figure 2 (a) illustrates the optical setup for a representative shock tube experiment. Although only one laser is shown in Fig. 2(a), often two lasers were coaligned through a single optical port to increase the information gathered per shock wave generated. Although only one optical path is shown in Fig. 2(a), each shock tube facility had six optical ports providing three beam paths. Across both shock tubes, zinc selenide windows were used for light in the 10-12 µm region and sapphire windows were used for light in the 3-4 µm region. In the 3-4 µm region, thermoelectrically-cooled Interband Cascade Lasers (ICL) were used for 3.1758 µm, 3.17595 µm, 3.283 µm, and 3.41 µm, and a He-Ne gas laser was used for 3.392 µm. For all new 10-12 µm cross-section measurements, a water-cooled CO_2 gas laser was used for 10.532 µm and 10.675 µm and an ethylene gycol mixture-cooled EC-QCL was used for 10.958 µm and 11.345 µm. The lasers were aligned through the measurement plane of each shock tube and onto photovoltaic detectors on the opposing side. Before detection, all beam paths were spatially filtered using irises and spectrally filtered using narrow-bandpass filters to mitigate signal from thermal emission of the test gas. Lasers in the 3-4 µm region were coupled with liquid nitrogen-cooled indium antimonide detectors and lasers in the 10-12 µm region with thermoelectrically-cooled mercury cadmium telluride detectors. A spectrum analyzer was used to check the wavelengths of all lasers before and after each experiment.

3. Multi-species, multi-wavelength laser absorption diagnostics

3.1. Vectorized and constrained Beer-Lambert systems

Multiple fixed-wavelength lasers can be used to probe the spectrum of a rapidly-reacting mixture to determine its time-resolved composition. Procedurally, this process involves calculation of the most likely combination of species that could create the discretely measured spectrum after taking the spectra of candidate species and physical system constraints (such as enforcing positive mole fractions) into consideration. An optimization framework to calculate the time-resolved composition will be presented here by introducing a

vectorized Beer-Lambert system, discussing system constraints and convexity, and presenting requirements of the absorption cross-section matrix.

When multiple species are considered, absorbance contributions from individual species sum linearly and Beer-Lambert relation can be expanded. Eq. 2 provides the expanded Beer-Lambert relation, which provides the total absorbance of a gas mixture of N species at wavelength λ.

$$\alpha_\lambda = \sum_{i=1}^{N} {}_{i,\lambda}(T,P) n_i L \tag{2}$$

When multiple wavelengths are considered, Eq. 2 can be further expanded into a system of equations and unknown mole fractions (x_i) as shown in Eq. 3. The set of equations in Eq. 3 is defined at each point in time and characterizes a system of N species using M wavelengths. In principle, if N species are present in a gas mixture, at least N wavelengths can be used for complete speciation.

$$\begin{aligned} {}_{CH4,\lambda_1} x_{CH4} + {}_{C2H4,\lambda_1} x_{C2H4} + \cdots {}_{N,\lambda_1} x_N &= \frac{\alpha_{\lambda_1}}{nL} \\ {}_{CH4,\lambda_2} x_{CH4} + {}_{C2H4,\lambda_2} x_{C2H4} + \cdots {}_{N,\lambda_2} x_N &= \frac{\alpha_{\lambda_2}}{nL} \\ \vdots & \\ {}_{CH4,M} x_{CH4} + {}_{C2H4,M} x_{C2H4} + \cdots {}_{N,\lambda_M} x_N &= \frac{\alpha_{\lambda_M}}{nL} \end{aligned} \tag{3}$$

A cross-section matrix $\{\mathrm{K} \in \mathbb{R}^{\mathrm{M}\times\mathrm{N}}\}$ (m^2 mol^{-1}), mole fraction vector $\{\vec{x} \in \mathbb{R}^{\mathrm{N}}\}$, and normalized absorbance vector $\{\vec{b} \in \mathbb{R}^{\mathrm{M}} \mid \vec{b} = \vec{\alpha}/nL\}$ (m^2 mol^{-1}) are established to vectorize the Beer-Lambert system of Eq. 3 into the form of Eq. 4.

$$\mathrm{K}\vec{x} = \vec{b} \tag{4}$$

Given K and $\vec{b}$, the mole fractions can be readily calculated. For determinant systems, if $M = N$, an analytical solution for $\vec{x}$ exists. However, Eq. 4 must be reformulated if the system is over-determined or constraints on the solution space are imposed. Eq. 4 is reformulated using the objective function provided in Eq. 5, which uses the squared l2 norm, as standard for regression. The objective function is strongly convex and of the same format as a least squares regression problem. Of note, the objective function of Eq. 5 should only be used on homoscedastic systems - a system where all residuals ($K\vec{x} - \vec{b}$) are expected to be of comparable magnitude.

$$Minimize: \left\| \mathrm{K}\vec{x} - (\vec{b}) \right\|_2^2 \tag{5}$$

Eq. 5 can also be solved subject to constraints, given that all constraints are also convex. System constraints provide a mathematical method to enforce physical solutions that must be upheld for any calculated mole fractions. Suggested system constraints are: (1) $\vec{x} \geq \mathbf{0}$, (2) the total number of atoms in the system must be less than or equal to the known amount at time-zero, and (3) $K\vec{x} \leq \vec{b}$. The third constraint enforces that the sum of the absorbance contribution from each species must not exceed the measured absorbance at each wavelength. Additional constraints can be implemented; however new constraints must maintain system convexity. Eq. 5 under the given constraints can be solved using a standard convex optimization solving platform, such as CVX developed by CVX Research Inc. [38-39], and implemented using Matlab software. To implement Eq. 5 using a numerical solver such as CVX, monotonicity in the nonlinear composition must be upheld. A modified objective function that is mathematically equivalent to Eq. 5, but complies with the numerical solver, is provided in Eq. 6. Mathematical equivalency is upheld because a norm, by definition, is positive.

$$Minimize\text{:}\ \max\left\{0\ ,\ \left\|\mathrm{K}\vec{x}-(\vec{b})\right\|_2\right\}^2 \qquad (6)$$

The simplicity in Eq. 6 belies the challenge associated with its implementation, which is mainly associated with the preparation of the absorption cross-section matrix K. The cross-section matrix K must be known *a priori* to enable calculation of mole fractions. At each point in time, and at a given pressure and temperature, $M \times N$ absorption cross-sections values are needed to populate matrix K. Furthermore, due to the temperature- and occasional pressure-dependency of each cross-section, in reality $M \times N$ *correlations* are needed to support each element of the matrix. Many supporting experiments are needed to construct each cross-section correlation used.

3.2. Determination of the temperature profile during pyrolysis

The temperature dependence of the cross-section matrix requires knowledge of a temperature time-history for any reactive gas mixture being studied. The temperature can either be measured directly or estimated using a chemical kinetics model. Normally, a modeled temperature profile is used [29,31,40-42].

3.3. Conditioning of the absorption cross-section matrix

Assuming all absorbers are accounted for, at least N linearly-independent rows and columns of the cross-section matrix are required to resolve N species. That is, all species cross-sections at one wavelength cannot be a scalar multiple of all cross-sections at any another wavelength. Likewise, across different species, the spectrum of one species cannot not be a scalar multiple of the spectrum of another species. Furthermore, the extent to which the rows and columns of the cross-section matrix differ (the condition number) is important to minimizing numerical error. To illustrate, Fig. 3 shows the spectra of C_3H_6 and 1-C_4H_8 in the 3-4 µm and 10-12 µm regions. If C_3H_6 and 1-C_4H_8 are the only species present, two wavelengths are sufficient, in principle, to solve the system. If both wavelengths are in the same narrow region of the spectra there is a risk of large numerical error due to small differences in the relative values of the two spectra. In any one spectral region, 1-C_4H_8 and C_3H_6 are nearly scalar multiples of the other. However, across different spectral regions, the species have an inverse relationship which can be leveraged. A prudent measurement of both 1-butene and propene will use both regions to ensure a well-conditioned cross-section matrix.

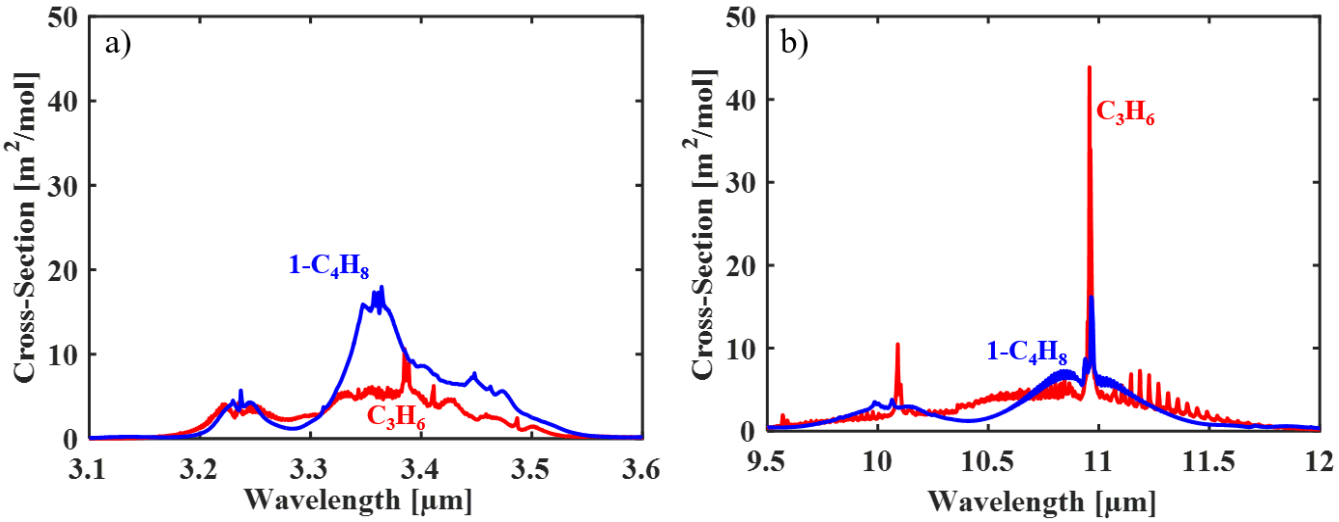

Fig. 3: An example of the overlapping spectra of C_3H_6 and 1-C_4H_8 at 323 K taken from PNNL spectral database [6] in (a) the 3-4 µm region, and (b) the 10-12µm region.

3.4. Heteroscedastic systems

A weighted objective function can be used for heteroscedastic systems, as shown in Eq. 7. An example of heteroscedasticity would be found in a system with overwhelming interfering absorbance at one wavelength but not others. Without using a weighted objective function, the optimization process will encounter artificially large squared error at the corrupted wavelength, which will disrupt the estimation of all mole fractions in order to minimize the disproportionately large squared error.

$$Minimize\text{: } \left\| W\left(\mathrm{K}\vec{x} - \left(\vec{b}\right)\right)\right\|_2^2 \tag{7}$$

Proper determination of the matrix $\{W \in \mathbb{R}^{\mathrm{M}\times\mathrm{N}} \mid W_{ij} = 0 \ if \ i \neq j \ and \ 0 \leq W_{ii} \leq 1 \ \forall \ i \in \{1,2,\dots,M\}\}$ will be discussed in a subsequent application of the current framework.

4. A review of species and wavelengths included

A brief review of fixed-wavelength infrared laser diagnostic systems is provided here for methane, ethylene, propene, 1-butene, iso-butene, benzene, toluene, and the four jet fuel samples. The species selected are characterized by their dominance during jet fuel pyrolysis according to recent kinetic models and flow reactor studies [12-13, 15]. While the discussion is limited to absorption spectra at temperatures above 1000 K, lower-temperature cross-sections from [43-47] were also aggregated and included in the final database to extend the domain of each cross-section correlation provided.

4.1. Methane | CH_4

Methane's importance in kinetic mechanisms, deleterious effect as a greenhouse gas, and high hydrogen-to-carbon ratio make it an important target of laser absorption diagnostic systems. Methane's presence in the pyrolysis of jet fuels warrants its inclusion in the current database. Among a diversity of infrared laser systems that have been used to study methane in the past quarter century [48-57], two fixed wavelengths at 3.1758 µm and 3.17595 µm were chosen as part of the current matrix approach. In 2015, Sur et al. [28] developed a two-wavelength, interference-free, and mid-IR methane diagnostic at 3.1758 µm and 3.17595 µm. To enable interference-free detection, Sur et al. used a two-color and peak-minus-valley subtraction technique that assumed all interfering absorbance varied weakly between the two wavelengths. When selecting a line, Sur et al. chose the peak absorption from a cluster of transitions in the R-branch of methane's ν_3 $^1A_1 \rightarrow {}^1F_2$ R(14) A, F, and E symmetry transitions. Notably, cross-section correlations for methane at 3.1758 µm and 3.17595 µm exhibit strong temperature and pressure-dependencies because they represent an amalgam of competing transitions.

Absorption cross-sections of methane at all other target wavelengths were included in the current database. However, only one other wavelength, 3.392 µm, showed strong absorption from methane. The absorption from methane at 3.392 µm has been studied extensively since 1970 using a helium-neon gas laser and included as part of the historical aggregation of data [20-27]. Notably, the absorption cross-section correlation provided at 3.392 µm demonstrates a strong pressure and temperature dependence because 3.392 µm coincides with a cluster of methane transitions.

While spectrally adjacent to 3.392 µm, another wavelength included in the database, 3.41 µm, has a very small methane cross-section. Deliberately by Wang et al. [26], the 3.41 µm laser diagnostic measures similar molecular vibrations as 3.392 µm (primarily, CH_3 degenerate stretch modes of large hydrocarbons) but with isolation from any methane transition. Although very small in magnitude, absorption cross-section data for methane at 3.41 µm from Wang et al. were included. New data for methane is also included from cross-section measurements at 3.283 µm and in the 10-12 µm region; although all methane absorption cross-section measurements were approximately zero in the 10-12 µm region.

4.2. Ethylene | C_2H_4

Ethylene is the dominant alkene formed during conventional jet fuel pyrolysis and holds great importance in the development of accurate kinetic mechanisms [14]. Furthermore, reactions involving ethylene are important for the formation of acetylene and, consequently, for the sooting propensity of a fuel [18]. Despite ethylene's importance in kinetic mechanisms, relatively few dedicated infrared laser diagnostics have been developed to measure ethylene formation from pyrolysis of larger hydrocarbons.

Since 1974, CO_2 gas lasers have been used to monitor ethylene in the 10-12 µm region. Before the turn of the century, Patty et al. [58], Persson et al. [59], and Olsen et al. [60] utilized the P14 line of a CO_2 laser (at 10.532 µm) to measure ethylene for very different applications, including ambient air sensing and laser-driven inertial-confinement fusion. More recently and pertaining to high-temperature gas phase chemistry, Pilla et al. [16] in 2011 and Haylett et al. [17] revisited the P14 line and published measurements of ethylene formation during n-heptane and diesel pyrolysis, respectively. The following year, Ren et al. [18] reported additional cross-section measurements at 10.532 µm and organized the initial work of Pilla et al. and Haylett et al. into a formal ethylene diagnostic, which has subsequently attracted extensive use in the literature. In 2013, MacDonald et al. [29] enhanced the 10.532 µm diagnostic by providing additional cross-sections at a nearby wavelength of 10.675 µm and demonstrating the use of an online/offline version of the original diagnostic. MacDonald et al. applied this online/offline ethylene diagnostic to support ethylene measurements during the pyrolysis of n-dodecane, methylcyclohexane, and iso-cetane. The online/offline ethylene diagnostic assumes the interference spectra of all absorbers are wavelength-independent between 10.532 µm and 10.675 µm. Recent measurements by Strand et al. [34] at 1000 K have shown this assumption to be approximately correct for many hydrocarbon species, though not all. For example, a candidate interfering species present in the decomposition of many large hydrocarbons is propene that was shown to have a slight difference in absorption cross-section between 10.532 µm and 10.675 µm. Appreciable amounts of propene may lead to artificially-low ethylene measurements if the online/offline method is used. In targeting propene afterwards, Chrystie et al. [30] in 2015 and Parise et al. [31] used EC-QCL lasers to provide more ethylene absorption cross-sections in the 10-12 µm region at 10.962 µm, 10.958 µm, and 10.953µm. Similarly, Spearrin et al. [19] provided ethylene cross-section data at 11.345 µm as part of a study on the interfering species of iso-butene. The current study provides more ethylene cross-section measurements at 11.345 µm to supplement the work of Spearrin et al.

In the 3-4 µm region, Sur et al. [28] included ethylene cross-sections in the development of the methane diagnostic at 3.1758 µm and 3.17595 µm. However, these cross-sections were not used with the online/offline two-color method. Although not previously used, there is information encoded in the interfering absorbance at both wavelengths, which can be leveraged when using a matrix method. Like most hydrocarbons, ethylene has also been studied extensively at 3.392 µm and 3.41 µm, and an aggregated cross-section dataset from literature is included for both wavelengths [20,23-27]. Ethylene has a small absorption cross-section at 3.392 µm and 3.41 µm due to an absence of CH_3 degenerate stretch modes that give most hydrocarbons strong absorbance at both wavelengths. In order to supplement the ethylene cross-sections in the literature, many new measurements are provided here for 3.1758 µm, 3.392 µm, and 3.41 µm, and 3.283 µm.

4.3. Propene | C_3H_6

The high thermal stability and abundance of propene following the decomposition of larger hydrocarbons make it an intermediate species of great interest in the proposed database. Although significant amounts of propene form during the pyrolysis of many fuels, its detection still presents a significant challenge. The dominant molecular vibrations of propene in the 3-4 µm region and 10-12 µm region are shared by many other molecules, which complicates any isolated measurements of propene among a blend of other hydrocarbons. For example, recent propene diagnostics developed by Chrystie et al. [30] and Parise et al. [31] measure absorption from an in-plane $=CH_2$ bending mode near 10.9 µm. However, the absorption spectra of 1-butene and 1,3-butadiene between 10 and 12 µm have been shown to be nearly scalar multiples of the spectrum of propene because of the same in-plane $=CH_2$ bending mode [34]. Therefore, it is possible to have interfering absorbance from molecules with spectra that are very similar to propene's spectrum in the 10-12 µm region. Interference spectra that have the same shape as propene can contribute to artificially high propene measurements unless a separate region of the spectra is used. The challenge associated with distinguishing between molecules with the same in-plane $=CH_2$ bending mode exemplifies a need for the proposed framework.

Despite the challenges associated with measuring propene, two recent studies have sought to identify propene among a blend. Chrystie et al. [30] and Parise et al. [31] detailed the development of two similar EC-QCL based propene diagnostics and associated cross-sections near 10.9 µm. Chrystie et al. provided a wealth of high-temperature cross-sections for a number of species at two wavelengths very close to propene's peak $=CH_2$ bending feature. The online/offline approach used by Chrystie et al. selected the two wavelengths of 10.962 µm and 10.89 µm and assumed that the spectra of all interfering species were constant across the online and offline wavelengths. Notably, Chrystie et al. validated this assumption for most candidate interfering species, with the exception of 1,3-butadiene. If 1,3-butadiene is expected to be present in large proportions, the online/offline method risks calculation of artificially-high propene mole fractions. Another two-wavelength propene method developed by Parise et al. reported a two-by-two matrix approach measuring propene and ethylene simultaneously at 10.532µm and 10.958 µm. The diagnostic of Parise et al. assumed that ethylene and propene were the only dominant species at each wavelength. The two-by-two matrix of ethylene and propene may be corrupted by the presence of other species besides ethylene and propene. Parise et al. provided a great number of absorption cross-sections at 10.958 µm to quantify candidate interfering species.

In addition to the studies of propene near 10.958 µm and 10.532 µm, propene cross-section measurements have been taken at other wavelengths to quantify its interference for other diagnostics. For example, in support of an iso-butene diagnostic, Spearrin et al. [19] provided propene cross-sections at 11.345 µm. Also included are cross-sections from the very recent high-temperature spectra covering 10.532µm, 10.675 µm, 10.89 µm, 10.96 µm, and 11.345 µm from Strand et al. [34]. In the 3-4µm region, cross-sections at 3.392 µm and 3.41 µm are available and included from the literature [20,23-27]. New propene cross-section measurements are provided as part of the current study at 3.1758 µm and 3.283 µm, 10.532 µm, 10.675 µm, and 11.345 µm.

4.4. Butene | C_4H_8

Isomers of butene have garnered recent attention due to their importance across a variety of kinetic models. Due to the highly paraffinic structure of alternative jet fuels, iso-butene is a dominant intermediate species during alternative jet fuel oxidation and commensurate in importance to ethylene for conventional jet fuels [11-12]. Another isomer, 1-butene, is a prominent species in reaction mechanisms for butanols, large alkanes, and conventional jet fuels [14,61]. Furthermore, scientific studies on butenes themselves, the smallest alkene with an isomeric structure, are invaluable in improving the fidelity of kinetic models [61-63]. Despite the importance of butenes, their kinetics are not yet well understood and limited laser diagnostics exist to-date for their detection. In 2014, Spearrin et al. [19] developed an innovative iso-butene diagnostic that used a pulsed EC-QCL at 11.345µm to probe iso-butene's in-plane $=CH_2$ bending vibrational mode. Due to the symmetric structure of iso-butene, vibrational dampening of the in-plane $=CH_2$ bending mode gives rise to a strong absorption feature that is at a slightly different wavelength than the similar mode of propene, 1-butene, and 1,3-butadiene. The distinct molecular vibration of iso-butene was leveraged by Spearrin et al. to measure iso-butene formation during iso-octane pyrolysis. While the absorption from other species was quantified at 11.345 µm, the single-wavelength iso-butene diagnostic does not account for interfering absorbance and may provide artificially high iso-butene measurements if any interfering species are present. Accordingly, inclusion of the iso-butene diagnostic at 11.345 µm into a broader matrix framework will improve its ability to resolve iso-butene by accounting for the presence of other absorbing species that contribute to the absorbance at 11.345 µm.

Besides existing measurements of iso-butene at 11.345 µm, other butene cross-sections have been measured by Chrystie et al. [30] and Parise et al. [31] at 10.89µm. 10.958 µm, and 10.96 µm. In the 3-4 µm region, butene cross-sections were available at 3.392 µm and 3.41 µm from the literature [23,26]. For iso-butene and 1-butene, a great number of new cross-section measurements were needed to complete the current database and new cross-section data are provided for all wavelengths, except for iso-butene at 3.41 µm. There exists no dedicated laser absorption study of 1-butene to-date besides historical studies of the absorption at 3.392 µm. Due to similarities in the spectra of other alkenes, 1-butene is not readily measured using any known online/offline technique. However, the proposed matrix method enables measurement of 1-butene and an ability to distinguish it among other alkenes. A subsequent study will provide the first application of the current multi-wavelength framework to 1-butene pyrolysis.

No absorption cross-section measurements of 2-butene are provided here and 2-butene has seen very limited discussion in the literature [61,64].

4.5. Benzene & Toluene | C_6H_6 C_7H_8

The formation of benzene and toluene during jet fuel pyrolysis provides valuable information about the lubricity, seal-swell characteristics, and coking predisposition of a fuel [65-66]. To the best of the authors' knowledge, and besides cross-section measurements as 3.392 µm, no infrared laser absorption diagnostic exists for aromatic molecules. Molecular vibrations of phenylated C-H bonds near 3.283 µm present an opportunity to measure aromatics species expected to be present in the high temperature pyrolysis of jet fuels and many other fuels. Accordingly, the wavelength of 3.283 µm was developed as part of the current study to include aromatics as part of a broader matrix method approach. The low-temperature absorption spectra of benzene and toluene are shown in Fig. 4 for the 3-4 µm region. Notably, the dashed black lines in Fig. 4 indicates the wavelengths included in the provided database.

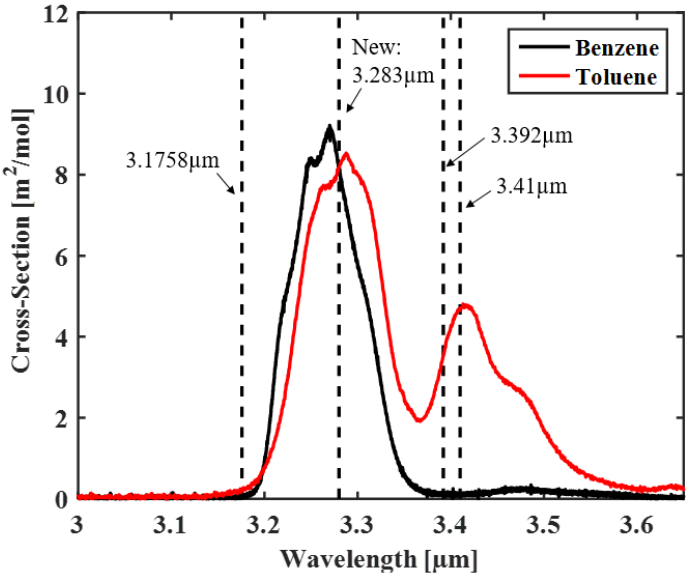

Fig. 4. Absorption cross-sections of benzene and toluene at 773 K [43]. The dashed lines indicate wavelengths included in the current database, with the new wavelength indicated.

4.6. Jet fuels: A1, A2, A3, and C1

High-temperature absorption cross-sections for four jet fuels referred to as A1 ($C_{10.8}H_{21.6}$), A2 ($C_{11.4}H_{21.7}$), A3 ($C_{12}H_{22.3}$), and C1 ($C_{12.5}H_{27.1}$) are included in the current database. The precise composition of each fuel is provided by a GCxGC analysis in the supplementary material. A1 is a sample of JP8, A2 of Jet A, A3 of JP5, and C1 of Gevo ATJ. The POSF codes for A1, A2, A3 and C1 are 10264, 10325, 10289, and 11498, respectively. The current study greatly expands upon previous cross-sections measured at 3.392 µm by Parise et al. [11,31] and Zhu [67]. New data is included at: 3.1758 µm, 3.283 µm, 10.532µm, 10.675 µm, 10.953 µm, and 11.345 µm as part of the current study. In addition to shock tube measurements of jet fuel, cross-sections are included in the 3-4 µm region up to 500 K from new FTIR measurements. The FTIR spectrometer used is detailed by Klingbeil et al. [43].

5. Absorption cross-section correlations

5.1. Description of database scope

We report absorption cross-sections at 3.1758µm, 3.17595µm, 3.283µm, 3.392µm, 3.41µm, 10.532µm, 10.675µm, 10.89µm, 10.958µm, 10.962µm, 11.345µm for the following small hydrocarbon species: methane (CH_4), ethylene (C_2H_4), propene (C_3H_6), iso-butene (i-C_4H_8), 1-butene (1-C_4H_8), benzene (C_6H_6), and toluene (C_7H_8). This work also provides high-temperature absorption cross-section measurements of three traditional fuels and one alternative fuel referred to here as A1, A2, A3, and C1. The current study has aggregated absorption cross-sections from the literature and provides hundreds of new high-temperature cross-section measurements from shock tube experiments.

Table 1 presents a summary of all of the absorption cross-section correlations included in this study. The cell values in Table 1 map to a cross-section correlation in Table 2. Table 2 presents absorption cross-section correlations based on new shock tube cross-section measurements as well as prior shock tube, FTIR, and broad-scan external cavity quantum cascade laser data aggregated from literature. In the supplemental material we provide a Matlab script that includes all correlations within a 95% confidence interval. The supplemental material also includes the data for each species at each wavelength. The temperature- and occasionally pressure-dependent cross-section correlations presented are empirical fits to the data. No pressure-dependence was observed for the majority of cases. In the case of an observed pressure-dependence (methane at 3.175 µm, 3.17595 µm, and 3.392 µm), a bivariate exponential was fitted to the data. No appreciable collision-partner dependency was observed in the data.

The residual squared error (RSS), sample number (n), and degrees of freedom (ν) are reported for all correlations. The degree of freedom was determined by the sample number reduced by the number of fit parameters for each correlation. We provide the necessary components for the calculation of a 95% confidence interval assuming the error in the cross-section value dominates for all cases. The 95% confidence interval around a predicted cross-section value is provided by $\pm U_\sigma$ where U_σ is defined in Equation 5 [68].

$$U_{\sigma,95\%} = t_{95\%}\left\{s_\sigma^2\left[\frac{1}{n}+\frac{(T-\bar{T})^2}{s_{TT}}\right]\right\}^{1/2} \tag{7}$$

s_σ, $T_{average}$, and s_{TT} are defined as:

$$s_\sigma = \sqrt{\frac{RSS}{\nu}} \tag{8}$$

$$\bar{T} = \frac{1}{n}\sum_{i=1}^{n} T_i \tag{9}$$

$$s_{TT} = \sum_{i=1}^{n} T_i^2 - \frac{(\sum_{i=1}^{n} T_i)^2}{n} \tag{10}$$

For pressure-dependent cross-section data the 95% confidence interval can be calculated using Eq. 9.

$$U_{\sigma,95\%} = t_{95\%}\left\{s_\sigma^2\left[\frac{1}{n}+\frac{(T-\bar{T})^2}{s_{TT}}+\frac{(P-\bar{P})^2}{s_{PP}}\right]\right\}^{1/2} \tag{11}$$

where $\bar{P}$ and s_{PP} are defined as:

$$\bar{P} = \frac{1}{n}\sum_{i=1}^{n} P_i \tag{12}$$

(13)

$$s_{PP} = \sum_{i=1}^{n} P_i^2 - \frac{(\sum_{i=1}^{n} P_i)^2}{n}$$

Table 1. Cross-section correlation reference table.

Wavelength	CH_4	C_2H_4	C_3H_6	iC_4H_8	$1C_4H_8$	C_6H_6	C_7H_8	A1	A2	A3	C1
3.1758 µm	1,1	1,2	1,3	1,4	1,5	1,6	1,7	1,8	1,9	1,10	1,11
3.17595 µm	2,1	2,2	2,3	2,4	2,5	2,6	2,7	2,8	2,9	2,10	2,11
3.283 µm	3,1	3,2	3,3	3,4	3,5	3,6	3,7	3,8	3,9	3,10	3,11
3.392 µm	4,1	4,2	4,3	4,4	4,5	4,6	4,7	4,8	4,9	4,10	4,11
3.41 µm	5,1	5,2	5,3	5,4	5,5	5,6	5,7	5,8	5,9	5,10	5,11
10.532 µm	6,1	6,2	6,3	6,4	6,5	6,6	6,7	6,8	6,9	6,10	6,11
10.675 µm	7,1	7,2	7,3	7,4	7,5	7,6	7,7	7,8	7,9	7,10	7,11
10.89 µm	8,1	8,2	8,3	8,4	8,5	8,6	8,7	8,8	8,9	8,10	8,11
10.958 µm	9,1	9,2	9,3	9,4	9,5	9,6	9,7	9,8	9,9	9,10	9,11
10.962 µm	10,1	10,2	10,3	10,4	10,5	10,6	10,7	10,8	10,9	10,10	10,11
11.345 µm	11,1	11,2	11,3	11,4	11,5	11,6	11,7	11,8	11,9	11,10	11,11

Table 2. Cross-section correlation table.

Species	***Cell***	***Fitted value of cross-section*** $(\sigma\ [\frac{m2}{mol}])$ ***vs. temperature*** $(T\ [K])$ ***in***	***Standard error*** $(n = \#\ of\ samples)$	***Reference***	***Notes and previous EQs that were used***
Cross-sections at 3.1758 μm					
CH_4	*1,1*	$= a_0 + a_1 \exp\left(-\frac{T - x_0}{b_1}\right) + a_2 \exp\left(-\frac{P}{b_2}\right)$ $a_0 = 0$ $a_1 = 85.43$ $a_2 = 37.28$ $b_1 = 342.64$ $b_2 = 0.487$ $x_0 = 711.96$	$n = 30$ $\nu = 25$ $RSS = 3.82E2$ $t_{95} = 2.06$ $s_{TT} = 4.054E6$ $\bar{T} = 1394$ $s_{PP} = 32.37$ $\bar{P} = 1.33$	*[28]*	*Methane exhibits a strong pressure dependence. Sur et al. [21] give the following correlation for the absorption coefficient in units of* $[cm^{-1}atm^{-1}]$*:* $k = \frac{6.562}{P}\exp(-81.95 - 0.7089 * lnP + 26.59lnT - 0.1216(lnP)^2 + 0.1836lnPlnT - 2.136(lnT)^2)$ *To derive use the relation:* $= \frac{k*T}{121.87}$ $[m^2/mol]$ *New correlation fit to:* $800 < T < 2200\ K$ $0.1 < P < 4\ atm$
C_2H_4	*1,2*	$= a_0 + a_1T + a_2T^2 + a_3T^3 + a_4T^4$ $a_0 = -1.28065$ $a_1 = 0.01415$ $a_2 = -2.13573E - 5$ $a_3 = 1.26315E - 8$ $a_4 = -2.6408E - 12$	$n = 22$ $\nu = 17$ $RSS = 0.257$ $t_{95} =$ $s_{TT} = 4.89E6$ $\bar{T} = 800$	*[43,46] & new*	*Correlation valid between 300-1800K.*
C_3H_6	*1,3*	$= a_0 + a_1T$ $a_0 = 0.43179$ $a_1 = (1.8598)E - 4$	$n = 15$ $\nu = 13$ $RSS = 0.102$ $t_{95} = 2.16$ $s_{TT} = 1.48E6$ $\bar{T} = 722.8$	*[43,45] & new*	*Correlation valid between 300-1400K.*
iC_4H_8	*1,4*	$= a_0 + a_1T$ $a_0 = 0.25772$ $a_1 = (1.02637)E - 4$	$n = 28$ $\nu = 25$ $RSS = 0.274$ $t_{95} = 2.06$ $s_{TT} = 9.005E6$ $\bar{T} = 975.8$	*new*	*Limited FTIR data. Shock tube data from the current study. Correlation valid between 600-1800K.*
$1C_4H_8$	*1,5*	$= a_0 + a_1 \exp\left(-\frac{T - x_0}{b_1}\right) + a_2 \exp\left(-\frac{T - x_0}{b_2}\right)$ $a_0 = 5.26$ $a_1 = -0.0042$ $a_2 = -4.563$ $b_1 = 162.27$ $b_2 = 14608.885$ $x_0 = 983.3$	$n = 21$ $\nu = 15$ $RSS = 0.120$ $t_{95} = 2.131$ $s_{TT} = 1.58E6$ $\bar{T} = 600$	*[43,44] & new*	*Correlation valid between 600-1300K.*
C_6H_6	*1,6*	$= a_0 + a_1 \exp\left(-\frac{T - x_0}{b_1}\right)$ $a_0 = 0.0156$ $a_1 = 1.478E - 4$ $x_0 = -592.84$ $b_1 = -228.7$	$n = 9$ $\nu = 5$ $RSS = 4.764E - 5$ $t_{95} = 2.571$ $s_{TT} = 250084$ $\bar{T} = 526$	*[43]*	*FTIR data from Klingbeil et al. [43] from 300-723 K used to extrapolate high-temperature correlation. Data is on the shoulder of a feature and exponential fit is appropriate.*
C_7H_8	*1,7*	$= a_0 + a_1 \exp\left(-\frac{T - x_0}{b_1}\right)$ $a_0 = 0.0819$ $a_1 = 1.184E - 4$ $x_0 = -1220.58$ $b_1 = -271$	$n = 11$ $\nu = 7$ $RSS = 0.0059$ $t_{95} = 2.365$ $s_{TT} = 260814$ $\bar{T} = 527$	*[43]*	*FTIR data from Klingbeil et al. [43] used to extrapolate high-temperature correlation. Data is on the shoulder of a feature and exponential fit is appropriate.*

A1	*1,8*	$= a_0 + a_1 \exp\left(-\frac{T - x_0}{b_1}\right)$ $a_0 = 0.341$ $a_1 = 6.158E-6$ $x_0 = -2260.35$ $b_1 = -283.25$	$n = 66$ $\nu = 62$ $RSS = 58.74$ $t_{95} = 2.00$ $s_{TT} = 1.06E7$ $\bar{T} = 990$	*new*	*Large uncertainty due to low absorbance and rapid fuel decomposition at high temperatures*
A2	*1,9*	$= a_0 + a_1 T$ $a_0 = -0.263$ $a_1 = (8.098)E-4$	$n = 38$ $\nu = 36$ $RSS = 14.83$ $t_{95} = 2.042$ $s_{TT} = 3.70E6$ $\bar{T} = 927$	*new*	*Large uncertainty due to low absorbance and rapid fuel decomposition at high temperatures*
A3	*1,10*	$= a_0 + a_1 T$ $a_0 = -0.0166$ $a_1 = 7.173E-4$	$n = 72$ $\nu = 70$ $RSS = 67.96$ $t_{95} = 2.00$ $s_{TT} = 6.04E6$ $\bar{T} = 962.3$	*new*	*Large uncertainty due to low absorbance and rapid fuel decomposition at high temperatures*
C1	*1,11*	$= a_0 + a_1 T$ $a_0 = -0.13292$ $a_1 = 0.00214$	$n = 12$ $\nu = 10$ $RSS = 0.464$ $t_{95} = 2.228$ $s_{TT} = 1.95E6$ $\bar{T} = 819$	*new*	*Large uncertainty due to low absorbance and rapid fuel decomposition at high temperatures*
Cross-sections at 3.17595 µm					
CH_4	*2,1*	$= a_0 + a_1 \exp\left(-\frac{T - x_0}{b_1}\right) + a_2 P$ $a_0 = 0$ $a_1 = 10.18$ $a_2 = 0.06877$ $b_1 = 934.53$ $x_0 = -23.32$	$n = 27$ $\nu = 23$ $RSS = 2.78$ $t_{95} = 2.069$ $s_{TT} = 2954184$ $\bar{T} = 1253$ $s_{PP} = 30.1227$ $\bar{P} = 1.41$	*[28] & new*	*Sur et al. [21] give the following correlation for the absorption coefficient in units of [$cm^{-1}atm^{-1}$]:* $k = \frac{7.022}{P}\exp(-14.78 + 5.298lnP + 5.491lnT + 0.09973(lnP)^2 - 0.5933lnPlnT - 0.5435(lnT)^2)$ *New correlation valid for:* $800 < T < 2200\ K$ $0.1 < P < 4\ atm$
C_2H_4	*1,2*	$= a_0 + a_1 T + a_2 T^2 + a_3 T^3 + a_4 T^4$ $a_0 = -1.28065$ $a_1 = 0.01415$ $a_2 = -2.13573E-5$ $a_3 = 1.26315E-8$ $a_4 = -2.6408E-12$	$n = 22$ $\nu = 17$ $RSS = 0.257$ $t_{95} =$ $s_{TT} = 4.89E6$ $\bar{T} = 800$	*[43,46] & new*	*Same as $_{1,2}$ because the absorbance of C_2H_4 is measured to be the same at 3148.81cm^{-1} and 3148.66cm^{-1}. Correlation valid between 300-1800K.*
C_3H_6	*1,3*	$= a_0 + a_1 T$ $a_0 = 0.43179$ $a_1 = (1.8598) * 10^{-4}$	$n = 15$ $\nu = 13$ $RSS = 0.102$ $t_{95} = 2.16$ $s_{TT} = 1.48E6$ $\bar{T} = 722.8$	*[43,45] & new*	*Same as $_{1,3}$ because the absorbance of C_2H_4 is measured to be the same at 3148.81cm^{-1} and 3148.66cm^{-1}. Correlation valid between 300-1400K.*
iC_4H_8	*1,4*	$= a_0 + a_1 T$ $a_0 = -0.04442$ $a_1 = (3.98493)E-4$	$n = 28$ $\nu = 25$ $RSS = 0.274$ $t_{95} = 2.06$ $s_{TT} = 9.005E6$ $\bar{T} = 975.8$	*new*	*Same as $_{1,4}$ because the absorbance of C_2H_4 is measured to be the same at 3148.81cm^{-1} and 3148.66cm^{-1}. Correlation valid between 600-1500K*

$1C_4H_8$	*1,5*	$= a_0 + a_1 \exp\left(-\frac{T - x_0}{b_1}\right) + a_2 \exp\left(-\frac{T - x_0}{b_2}\right)$ $a_0 = 5.26$ $a_1 = -0.0042$ $a_2 = -4.563$ $b_1 = 162.27$ $b_2 = 14608.885$ $x_0 = 983.3$	$n = 21$ $\nu = 15$ $RSS = 0.120$ $t_{95} = 2.131$ $s_{TT} = 1.58E6$ $\bar{T} = 600$	*[43,44] & new*	*Same as $_{1,5}$ because the absorbance of C_2H_4 is measured to be the same at 3148.81cm^{-1} and 3148.66cm^{-1}. Correlation valid between 600-1300K.*
C_6H_6	*1,6*	$= a_0 + a_1 \exp\left(-\frac{T - x_0}{b_1}\right)$ $a_0 = 0.0156$ $a_1 = 1.478E - 4$ $x_0 = -592.84$ $b_1 = -228.7$	$n = 9$ $\nu = 5$ $RSS = 2.095E - 4$ $t_{95} = 2.571$ $s_{TT} = 250084$ $\bar{T} = 526$	*[43]*	*Same as $_{1,6}$ because the absorbance of C_2H_4 is measured to be the same at 3148.81cm^{-1} and 3148.66cm^{-1}.*
C_7H_8	*1,7*	$= a_0 + a_1 \exp\left(-\frac{T - x_0}{b_1}\right)$ $a_0 = 0.0819$ $a_1 = 1.184E - 4$ $x_0 = -1220.58$ $b_1 = -271$	$n = 11$ $\nu = 7$ $RSS = 0.0059$ $t_{95} = 2.365$ $s_{TT} = 260814$ $\bar{T} = 527$	*[43]*	*Same as $_{1,7}$ because the absorbance of C_2H_4 is measured to be the same at 3148.81cm^{-1} and 3148.66cm^{-1}.*
A1	*1,8*	$= a_0 + a_1 \exp\left(-\frac{T - x_0}{b_1}\right)$ $a_0 = 0.341$ $a_1 = 6.158E - 6$ $x_0 = -2260.35$ $b_1 = -283.25$	$n = 66$ $\nu = 62$ $RSS = 58.74$ $t_{95} =$ $s_{TT} = 1.06E7$ $\bar{T} = 990$	*new*	*Same as $_{1,8}$ because the absorbance of C_2H_4 is measured to be the same at 3148.81cm-1 and 3148.66cm-1.*
A2	*1,9*	$= a_0 + a_1 T$ $a_0 = -0.263$ $a_1 = (8.098)E - 4$	$n = 38$ $\nu = 36$ $RSS = 14.83$ $t_{95} = 2.042$ $s_{TT} = 3.70E6$ $\bar{T} = 927$	*new*	*Same as $_{1,9}$ because the absorbance of C_2H_4 is measured to be the same at 3148.81cm-1 and 3148.66cm-1.*
A3	*1,10*	$= a_0 + a_1 T$ $a_0 = -0.0166$ $a_1 = 7.173E - 4$	$n = 72$ $\nu = 70$ $RSS = 67.96$ $t_{95} = 2.66$ $s_{TT} = 6.04E6$ $\bar{T} = 962.3$	*new*	*Same as $_{1,10}$ because the absorbance of C_2H_4 is measured to be the same at 3148.81cm-1 and 3148.66cm-1.*
C1	*1,11*	$= a_0 + a_1 T$ $a_0 = -0.072$ $a_1 = 0.00173$	$n = 20$ $\nu = 18$ $RSS = 3.018$ $t_{95} = 2.101$ $s_{TT} = 1.95E6$ $\bar{T} = 819$	*new*	*Same as $_{1,11}$ because the absorbance of C_2H_4 is measured to be the same at 3148.81cm-1 and 3148.66cm-1.*
Cross-sections at 3.283 μm					
CH_4	*3,1*	$= a_0 + a_1 T$ a_0 *=0.11986* $a_1 = -2.67281E - 5$	$n = 31$ $\nu = 29$ $RSS = 0.0316$ $t_{95} = 2.045$ $s_{TT} = 2.78E6$ $\bar{T} = 1177.41$	*[46] & new*	*Correlation valid between 300-1400K.*
C_2H_4	*3,2*	$= a_0 + a_1 \exp\left(-\frac{T - x_0}{b_1}\right)$ $a_0 = 1.663$ $a_1 = -0.531$ $x_0 = 302.119$ $b_1 = 86.317$	$n = 13$ $\nu = 9$ $RSS = 0.44169$ $t_{95} = 2.262$ $s_{TT} = 1.61E6$ $\bar{T} = 857.8$	*[43,46] & new*	*Correlation valid between 300-1550K.*

C_3H_6	*3,3*	$= a_0 + a_1T + a_2T^2 + a_3T^3$ $a_0 = -0.48357$ $a_1 = 0.01116$ $a_2 = -1.046E-5$ $a_3 = 3.035E-9$	$n = 15$ $\nu = 11$ $RSS = 0.05789$ $t_{95} = 2.201$ $s_{TT} = 1.55E6$ $\bar{T} = 726.9$	*[43,45] & new*	*Correlation valid between 300-1400K.*
iC_4H_8	*3,4*	$= a_0 + a_1T$ a_0 =*2.96049* $a_1 = 3.76558E-4$	$n = 6$ $\nu = 4$ $RSS = 0.0893$ $t_{95} = 2.776$ $s_{TT} = 4.55E5$ $\bar{T} = 1077$	*new*	*Small data set. Correlation valid between 300-1500K.*
$1C_4H_8$	*3,5*	$= a_0 + a_1T + a_2T^2 + a_3T^3 + a_4T^4$ $a_0 = 0.03407$ $a_1 = 0.00213$ $a_2 = 3.327E-6$ $a_3 = -8.731\,E-9$ $a_4 = 2.607\,E-12$	$n = 50$ $\nu = 45$ $RSS = 0.18317$ $t_{95} = 2.021$ $s_{TT} = 4.62E6$ $\bar{T} = 714.6$	*[43,44] & new*	*Correlation valid between 300-1500K.*
C_6H_6	*3,6*	$= a_0 + a_1 \exp\left(-\frac{T - x_0}{b_1}\right)$ $a_0 = 7.0305$ $a_1 = 4.66$ $x_0 = 293.274$ $b_1 = 193.89$	$n = 13$ $\nu = 9$ $RSS = 1.592$ $t_{95} = 2.262$ $s_{TT} = 1.42E6$ $\bar{T} = 697.16$	*[43] & new*	*Correlation valid between 300-1500K.*
C_7H_8	*3,7*	$= a_0 + a_1 \exp\left(-\frac{T - x_0}{b_1}\right)$ $a_0 = 7.7053$ $a_1 = 3.058$ $x_0 = 226.73$ $b_1 = 386.158$	$n = 16$ $\nu = 12$ $RSS = 0.729$ $t_{95} = 2.179$ $s_{TT} = 2.05E6$ $\bar{T} = 727$	*[43] & new*	*Correlation valid between 300-1600K.*
A1	*3,8*	$= a_0 + a_1 \exp\left(-\frac{T - x_0}{b_1}\right)$ $a_0 = 0.802$ $a_1 = 0.13412$ $x_0 = -476.58$ $b_1 = -433.70$	$n = 7$ $\nu = 3$ $RSS = 0.02871$ $t_{95} = 3.182$ $s_{TT} = 6.44E5$ $\bar{T} = 578.6$	*new*	*Correlation valid between 300-1400K.*
A2	*3,9*	$= a_0 + a_1T + a_2T^2 + a_3T^3$ $a_0 = -1.3009$ $a_1 = 0.01306$ $a_2 = -1.49931E-5$ $a_3 = 4.761E-9$	$n = 23$ $\nu = 19$ $RSS = 1.024$ $t_{95} = 2.093$ $s_{TT} = 2.44E6$ $\bar{T} = 860.6$	*new*	*Correlation valid between 300-1400K.*
A3	*3,10*	$= a_0 + a_1 \exp\left(-\frac{T - x_0}{b_1}\right)$ $a_0 = 5.672$ $a_1 = -4.0115$ $x_0 = 384.9$ $b_1 = 542.82$	$n = 13$ $\nu = 8$ $RSS = 0.55$ $t_{95} = 2.306$ $s_{TT} = 2.08E6$ $\bar{T} = 755$	*new*	*Correlation valid between 300-1400K.*
C1	*3,11*	$= a_0 + a_1T$ $a_0 = -0.497$ $a_1 = 0.00295$	$n = 21$ $\nu = 19$ $RSS = 22.4$ $t_{95} = 2.093$ $s_{TT} = 2.42E6$ $\bar{T} = 917.6$	*new*	*Correlation valid between 300-1400K.*
Cross-sections at 3.39µm					

CH_4	*4,1*	$= a_0 + a_1 \exp\left(-\frac{T - x_0}{b_1}\right) + a_2 \exp\left(-\frac{P}{b_2}\right)$ $a_0 = 0.66$ $a_1 = 27.92$ $a_2 = 40.35$ $x_0 = 291.59$ $b_1 = 354.39$ $b_2 = 0.35$	$n = 121$ $\nu = 115$ $RSS = 8.134E3$ $t_{95} = 1.98$ $s_{TT} = 2.561E7$ $\bar{T} = 906$ $s_{PP} = 54.8563$ $\bar{P} = 0.894$ *Although nearly 300 measurements were found in the literature, only 120 measurements explicitly listed the pressure.*	*[20-27,43,46]*	*Wang et al. [26] give the following relation in units of [m^2/mol]:* $= 1.66\text{E}11\text{P}^{-0.72}\text{T}^{-3.24} \exp\left(-\frac{1350}{\text{T}}\right)$ *Nativel et al. [27] gives the following relation in units of [m^2/mol] all measured at ~1.8atm:* $= 1.44 + (50.91 * 0.9976^{\text{T}})$ *Hidaka [23] gives the following relations in units of [cm^2/mol] for the decadic absorption cross-section:* $= (3.844E4) - 18.7T \; if \; T < 1500K$ $= (1.33E4) - 2.2T \; if \; T < 1500K$ *Correlation valid between 300-2500K.*
C_2H_4	*4,2*	$= a_0 + a_1 T + a_2 T^2 + a_3 T^3$ $a_0 = 0.2517$ $a_1 = 0.00131$ $a_2 = -9.48685E-7$ $a_3 = -2.50727E-10$	$n = 127$ $\nu = 123$ $RSS = 3.6275$ $t_{95} = 1.98$ $s_{TT} = 2.70E7$ $\bar{T} = 1069$	*[20,23-27,43,46] & new*	*Wang et al. [26] give the following relation in units of [m^2/mol]:* $\left[\frac{m^2}{mol}\right] = 0.94 + 1.25 \times 10^{-4}\text{T}$ *Olson et al. [20] give the following relation in units of [cm^2/mol](with absorbance defined by log10):* $_{10}\left[\frac{cm^2}{mol}\right] = (4.0 \pm 0.1) * 10^3$ *Koike et al. [24] give the following relations in units of [cm^2/mol] for the decadic absorption cross-section:* $_{10} * \left[\frac{cm^2}{mol}\right] = (0.96 \pm 0.37) * 10^3 + (1.99 \pm 0.27)T$ *Hidaka [23] gives the following relations in units of [cm^2/mol] for the decadic absorption cross-section:* $= 3.375 * T$ *Correlation valid between 300-2250K.*
C_3H_6	*4,3*	$= a_0 + a_1 \exp\left(-\frac{T - x_0}{b_1}\right)$ $a_0 = 33556.16$ $a_1 = -12191.824$ $x_0 = -1.769E7$ $b_1 = -1.747E7$	$n = 101$ $\nu = 97$ $RSS = 18.06$ $t_{95} = 2.00$ $s_{TT} = 2.65E7$ $\bar{T} = 1217$	*[24,26,43,45] & new*	*Wang et al. [26] give the following relation in units of [m^2/mol]:* $\left[\frac{m^2}{mol}\right] = 6.35 - 1.71\text{E} - 3\text{T}$ *Koike et al. [24] give the following relations in units of [cm^2/mol] for the decadic absorption cross-section:* $_{10} * \left[\frac{cm^2}{mol}\right] = (2.38 \pm 0.07) * 10^4 + (-6.70 \pm 0.49)T$ *Correlation valid between 300-2300K.*
iC_4H_8	*4,4*	$= a_0 + a_1 T$ $a_0 = 12.888$ $a_1 = (-0.00461)$	$n = 25$ $\nu = 23$ $RSS = 9.224$ $t_{95} = 2.069$ $s_{TT} = 2.59E6$ $\bar{T} = 996.3$	*[26] & new*	*Wang et al. [26] give the following relation in units of [m^2/mol]:* $\left[\frac{m^2}{mol}\right] = 15.36 - 9.09 \times 10^{-3}\text{T} + 2.10 \times 10^{-6}\text{T}^2$ *Correlation valid between 300-1700K.*

$1C_4H_8$	*4,5*	$= a_0 + a_1 \exp\left(-\frac{T - x_0}{b_1}\right) + a_2 \exp\left(-\frac{T - x_0}{b_2}\right)$ $a_0 = 6.7365$ $a_1 = -2.3187$ $a_2 = 2.85$ $b_1 = 452.106$ $b_2 = 473.538$ $x_0 = 2248.015$	$n = 48$ $\nu = 42$ $RSS = 12.505$ $t_{95} = 2.021$ $s_{TT} = 4.28E6$ $\bar{T} = 894.8$	*[26,43-44] & new*	*Wang et al. [26] give the following relation in units of [m^2/mol]:* $\left[\frac{m^2}{mol}\right] = 12.36 - 2.25\text{E} - 3\text{T}$ *Correlation valid between 300-1700K.*
C_6H_6	*4,6*	$= a_0 + a_1 \exp\left(-\frac{T - x_0}{b_1}\right)$ $a_0 = 0.03117$ $a_1 = 6.325E - 4$ $x_0 = 340.39$ $b_1 = -93.59815$	$n = 9$ $\nu = 5$ $RSS = 9.90E - 5$ $t_{95} = 2.571$ $s_{TT} = 2.50E5$ $\bar{T} = 526.42$	*[43]*	*Correlation valid between 300-800K.*
C_7H_8	*4,7*	$= a_0 + a_1 \exp\left(-\frac{T - x_0}{b_1}\right)$ $a_0 = 3.425$ $a_1 = 1.681$ $x_0 = 333.2$ $b_1 = 215.36$	$n = 29$ $\nu = 25$ $RSS = 2.708$ $t_{95} =$ $s_{TT} = 3.30E6$ $\bar{T} = 820.45$	*[43] & new*	*Correlation valid between 300-1600K.*
A1	*4,8*	$= a_0 + a_1 T + a_2 T^2 + a_3 T^3$ $a_0 = 35.84$ $a_1 = 0.0426$ $a_2 = -2.714E - 5$ $a_3 = -5.11E - 9$	$n = 95$ $\nu = 91$ $RSS = 454.46$ $t_{95} = 2.00$ $s_{TT} = 7.57E6$ $\bar{T} = 967.6$	*[67] & new*	*Correlation valid between 300-1400K.*
A2	*4,9*	$= a_0 + a_1 T + a_2 T^2 + a_3 T^3$ $a_0 = 54.89$ $a_1 = -0.03$ $a_2 = 4.933E - 5$ $a_3 = -3.136E - 8$	$n = 39$ $\nu = 35$ $RSS = 270.06$ $t_{95} = 2.042$ $s_{TT} = 3.85E6$ $\bar{T} = 937.1$	*[67] & new*	*Correlation valid between 300-1400K.*
A3	*4,10*	$= a_0 + a_1 T + a_2 T^2 + a_3 T^3$ $a_0 = 52.82$ $a_1 = -0.011$ $a_2 = 3.65E - 5$ $a_3 = -3.086E - 8$	$n = 72$ $\nu = 68$ $RSS = 696.3$ $t_{95} = 2.00$ $s_{TT} = 6.04E6$ $\bar{T} = 962.3$	*[67] & new*	*Correlation valid between 300-1400K.*
C1	*4,11*	$= a_0 + a_1 T + a_2 T^2 + a_3 T^3$ $a_0 = 85.26$ $a_1 = -0.095$ $a_2 = 1.806E - 4$ $a_3 = -1.0595E - 7$	$n = 23$ $\nu = 19$ $RSS = 97.83$ $t_{95} = 2.093$ $s_{TT} = 2.49E6$ $\bar{T} = 901.8$	*[67]& new*	*Correlation valid between 300-1400K.*
Cross-sections at 3.41 µm					
CH_4	*5,1*	$= a_0 + a_1 T$ $a_0 =$*-0.056* $a_1 = 5.68E - 4$	$n = 33$ $\nu = 31$ $RSS = 0.7906$ $t_{95} = 2.042$ $s_{TT} = 5.43E6$ $\bar{T} = 992.8$	*[26,43,46]*	*Relation from Wang et al. [26]:* $= 0.14 + 4.51 \times 10^{-4} T$ *Correlation valid between 300-1700K.*
C_2H_4	*5,2*	$= a_0 + a_1 \exp\left(-\frac{T - x_0}{b_1}\right)$ $a_0 = 1.1289$ $a_1 = -1.149$ $x_0 = 275.07$ $b_1 = 281.4$	$n = 26$ $\nu = 22$ $RSS = 0.085$ $t_{95} = 2.074$ $s_{TT} = 3.86E6$ $\bar{T} = 842.4$	*[26,43,46]*	Relation from Wang et al. [26]: $= 0.85 + 1.57 \times 10 - 4 T$ *Correlation valid between 300-1600K.*

C_3H_6	*5,3*	$= a_0 + a_1 \exp\left(-\frac{T - x_0}{b_1}\right)$ $a_0 = 3.09$ $a_1 = 1.96$ $x_0 = 407.8$ $b_1 = 658.84$	$n = 39$ $\nu = 35$ $RSS = 5.27$ $t_{95} = 2.042$ $s_{TT} = 4.00E6$ $\bar{T} = 736.4$	*[26,43,45]*	Wang et al. [26]: $= 4.74 - 8.09 \times 10^{-4}\, T$ *Correlation valid between 300-1650K.*
iC_4H_8	*5,4*	$= a_0 + a_1 T + a_2 T^2 + a_3 T^3$ $a_0 = 4.04916$ $a_1 = 0.01297$ $a_2 = -1.15281E - 5$ $a_3 = 2.73625E - 9$	$n = 16$ $\nu = 12$ $RSS = 0.07024$ $t_{95} = 2.179$ $s_{TT} = 1.48E6$ $\bar{T} = 991.8$	*[26]*	Relation from Wang et al. [26]: $\sigma = 4.05 + (1.30E-2)T - (1.16E-5)T^2 + (2.79E-9)T^3$ *Correlation valid between 300-1600K.*
$1C_4H_8$	*5,5*	$= a_0 + a_1 T + a_2 T^2 + a_3 T^3$ $a_0 = 6.942$ $a_1 = 0.00164$ $a_2 = 3.563E - 6$ $a_3 = -2.751E - 9$	$n = 22$ $\nu = 18$ $RSS = 0.35393$ $t_{95} = 2.101$ $s_{TT} = 2.39E6$ $\bar{T} = 785.9$	*[26,43,44] & new*	Relation from Wang et al. [26]: $= 9.36 - (5.03E-3)T + (9.67E-6)T^2 - (4.58E-9)T^3$ *Correlation valid between 300-1600K.*
C_6H_6	*5,6*	$= a_0 + a_1 T$ $a_0 = -0.0317$ $a_1 = 1.90408E - 4$	$n = 9$ $\nu = 7$ $RSS = 0.00106$ $t_{95} = 2.365$ $s_{TT} = 2.5E5$ $\bar{T} = 526.4$	*[43]*	*Correlation valid between 300-800K.*
C_7H_8	*5,7*	$= a_0 + a_1 \exp\left(-\frac{T - x_0}{b_1}\right)$ $a_0 = 2.7203$ $a_1 = 3.757$ $x_0 = 336.59$ $b_1 = 590.19$	$n = 23$ $\nu = 19$ $RSS = 1.9796$ $t_{95} = 2.093$ $s_{TT} = 2.19E6$ $\bar{T} = 747.8$	*[43]*	*Correlation valid between 300-1400K.*
A1	*5,8*	$= a_0 + a_1 T$ $a_0 = 98.75$ $a_1 = -0.0534$	$n = 6$ $\nu = 4$ $RSS = 0.53578$ $t_{95} = 2.776$ $s_{TT} = 3.36E4$ $\bar{T} = 458$	*new*	*Correlation valid between 300-600K.*
A2	*5,9*	$= a_0 + a_1 \exp\left(-\frac{T - x_0}{b_1}\right)$ $a_0 = -37.15$ $a_1 = 83.56$ $x_0 = 1041.76$ $b_1 = 2294.5$	$n = 12$ $\nu = 8$ $RSS = 23.62$ $t_{95} = 2.306$ $s_{TT} = 1.43E6$ $\bar{T} = 624.3$	*new*	*Correlation valid between 300-1400K.*
A3	*5,10*	$= a_0 + a_1 T$ $a_0 = 95.56$ $a_1 = -0.048$	$n = 8$ $\nu = 6$ $RSS = 1.33$ $t_{95} = 2.447$ $s_{TT} = 6.71E5$ $\bar{T} = 600$	*new*	*Correlation valid between 300-1400K.*
C1	*5,11*	$= a_0 + a_1 T + a_2 T^2 + a_3 T^3$ $a_0 = 42.79$ $a_1 = -0.055$ $a_2 = 1.542E - 4$ $a_3 = -9.1854E - 8$	$n = 15$ $\nu = 11$ $RSS = 8.76$ $t_{95} = 2.201$ $s_{TT} = 1.91E6$ $\bar{T} = 650$	*new*	*Correlation valid between 300-1400K.*
Cross-sections at 10.532 μm					
CH_4	*6,1*	*Approximately Zero*		*[6]*	*Approximately Zero*

C_2H_4	6,2	$= a_0 + a_1 \exp\left(-\frac{T - x_0}{b_1}\right) + a_2 \exp\left(-\frac{T - x_0}{b_2}\right)$ $a_0 = 5.597$ $a_1 = 44.04$ $a_2 = 42.30$ $b_1 = 259.77$ $b_2 = 259.792$ $x_0 = 370.56$	$n = 112$ $\nu = 106$ $RSS = 569.88$ $t_{95} = 1.98$ $s_{TT} = 1.71E7$ $\bar{T} = 1092$	*[16,18,29,34,67] & new*	*Ren et al. [18] Relation:* $= a_0 + a_1 \exp\left(-\frac{T}{b_1}\right) + a_2 \exp\left(-\frac{T}{b_2}\right)$ $a_0 = 4.8,\ a_1 = 383.7,\ a_2 = 103.5,$ $b_1 = 183,\ b_2 = 378.8$ *This work adds data to the Ren data and provides a new relation and uncertainty.* *Correlation valid between 400-2000K.*
C_3H_6	6,3	$= a_0 + a_1 \exp\left(-\frac{T - x_0}{b_1}\right)$ $a_0 = 2.39$ $a_1 = 2.137$ $x_0 = 486.75$ $b_1 = 534.63$	$n = 15$ $\nu = 11$ $RSS = 0.14819$ $t_{95} = 2.201$ $s_{TT} = 2.18E6$ $\bar{T} = 1103$	*[34] & new*	*Correlation valid between 400-1750K.*
iC_4H_8	6,4	$= a_0 + a_1 T$ $a_0 = -0.3$ $a_1 = 0.00105$	$n = 21$ $\nu = 19$ $RSS = 0.85959$ $t_{95} = 2.093$ $s_{TT} = 1.61E6$ $\bar{T} = 1076$	*new*	*y-intercept was fixed by the author.* *Correlation valid between 650-1600K.*
$1C_4H_8$	6,5	$= a_0 + a_1 \exp\left(-\frac{T - x_0}{b_1}\right)$ $a_0 = 3.143$ $a_1 = -1.423$ $x_0 = 299.26$ $b_1 = 88.08$	$n = 20$ $\nu = 16$ $RSS = 0.3207$ $t_{95} = 2.120$ $s_{TT} = 2.90E6$ $\bar{T} = 795.6$	*[44] & new*	*Correlation valid between 300-1400K.*
C_6H_6	6,6	*Approximately zero*		*[6]*	*Approximately zero*
C_7H_8	6,7	$= a_0 + a_1 T$ $a_0 = 0$ $a_1 = 3.69E - 4$	$n = 3$ $\nu = 2$ $RSS = 0.426$ $t_{95} = 4.303$ $s_{TT} = 3.93E4$ $\bar{T} = 13801$	*new*	*y-intercept was set by the author. Large uncertainty. Correlation valid between 1200-1400K.*
A1	6,8	$= a_0 + a_1 T$ $a_0 = -3.03494$ $a_1 = 0.00363$	$n = 44$ $\nu = 42$ $RSS = 193.248$ $t_{95} = 2.021$ $s_{TT} = 2.74E6$ $\bar{T} = 990.2$	*new*	*Large uncertainty. Correlation valid between 300-1400K.*
A2	6,9	$= a_0 + a_1 T$ $a_0 = -0.68632$ $a_1 = (0.00109)$	$n = 10$ $\nu = 8$ $RSS = 1.0747$ $t_{95} = 2.306$ $s_{TT} = 6.96E5$ $\bar{T} = 1053$	*new*	*Large uncertainty. Correlation valid between 300-1400K.*
A3	6,10	$= a_0 + a_1 T$ $a_0 = 0.386$ $a_1 = 2.617E - 4$	$n = 36$ $\nu = 34$ $RSS = 5.606$ $t_{95} = 2.042$ $s_{TT} = 2.41E6$ $\bar{T} = 1014$	*new*	*Large uncertainty. Correlation valid between 300-1400K.*
C1	6,11	$= a_0 + a_1 T$ $a_0 = 0$ $a_1 = 3.32E - 4$	$n = 7$ $\nu = 6$ $RSS = 22.13$ $t_{95} = 2.447$ $s_{TT} = 4.34E5$ $\bar{T} = 1014$	*new*	*Large uncertainty. Y-intercept was set by the author. Correlation valid between 300-1400K.*
Cross-sections at 10.675μm					
CH_4	7,1	*Approximately zero*		*[6]*	*Approximately zero*

C_2H_4	7,2	$= a_0 + a_1 T$ $a_0 = 3.13$ $a_1 = 5.36E-4$	$n = 60$ $\nu = 59$ $RSS = 6.66539$ $t_{95} = 2.000$ $s_{TT} = 5.26E6$ $\bar{T} = 984.5$	*[29,34,67] & new*	*McDonald et al. [29]:* $= 4$ *y-intercept fixed by author. Correlation valid between 500-1600K.*
C_3H_6	7,3	$= a_0 + a_1 T$ $a_0 = 5$ $a_1 = -4.37E-4$	$n = 7$ $\nu = 6$ $RSS = 5.54712$ $t_{95} = 2.447$ $s_{TT} = 7.04E5$ $\bar{T} = 955.0$	*[34] & new*	*Large uncertainty. y-intercept fixed by the author. Correlation valid between 400-1400K.*
iC_4H_8	7,4	$= a_0 + a_1 T$ $a_0 = 1.1$ $a_1 = 2.36E-4$	$n = 7$ $\nu = 5$ $RSS = 0.33878$ $t_{95} = 2.571$ $s_{TT} = 9.49E5$ $\bar{T} = 1081$	*new*	*Correlation valid between 700-1600K.*
$1C_4H_8$	7,5	$= a_0 + a_1 T$ $a_0 = 4.378$ $a_1 = -0.0011$	$n = 16$ $\nu = 14$ $RSS = 0.86252$ $t_{95} = 2.145$ $s_{TT} = 1.97E6$ $\bar{T} = 755.811$	*[34,44] & new*	*Correlation valid between 300-1400K.*
C_6H_6	7,6	*Approximately zero*		*[6]*	*Approximately zero*
C_7H_8	7,7	*Approximately zero*		*[6]*	*Approximately zero*
A1	7,8	$= a_0 + a_1 T$ $a_0 = 1.52294$ $a_1 = (9.54376)E-4$	$n = 22$ $\nu = 20$ $RSS = 71.86$ $t_{95} = 2.086$ $s_{TT} = 1.47E6$ $\bar{T} = 1000$	*new*	*Large uncertainty. Correlation valid between 300-1400K.*
A2	7,9	$= a_0 + a_1 T$ $a_0 = -1.354$ $a_1 = (0.00204)$	$n = 22$ $\nu = 20$ $RSS = 6.0704$ $t_{95} = 2.086$ $s_{TT} = 1.38E6$ $\bar{T} = 998$	*new*	*Large uncertainty. Correlation valid between 300-1400K.*
A3	7,10	$= a_0 + a_1 T$ $a_0 = 0.674$ $a_1 = (-1.547)E-4$	$n = 29$ $\nu = 27$ $RSS = 2.75118$ $t_{95} = 2.052$ $s_{TT} = 8.99E5$ $\bar{T} = 1001$	*new*	*Large uncertainty. Correlation valid between 300-1400K.*
C1	7,11	$= a_0 + a_1 T$ $a_0 = 0$ $a_1 = 0.00279$	$n = 8$ $\nu = 7$ $RSS = 28.68$ $t_{95} = 2.365$ $s_{TT} = 4.78E5$ $\bar{T} = 983.64$	*new*	*Large uncertainty. Y-intercept fixed by the author. Correlation valid between 300-1400K.*
Cross-sections at 10.89 μm					
CH_4	8,1	*Approximately zero*		*[6]*	*Approximately zero*
C_2H_4	8,2	$= a_0 + a_1 T$ $a_0 = 2.238$ $a_1 = (-3.33)E-5$	$n = 7$ $\nu = 5$ $RSS = 0.01691$ $t_{95} = 2.571$ $s_{TT} = 9.87E5$ $\bar{T} = 1417$	*[30]*	*Measured to be approximately the same as (10,2). Correlation fit to the combined data of (8,2) and (10,2). Correlation valid between 900-1900K.*

C_3H_6	*8,3*	$= a_0 + a_1 T$ $a_0 = 5.26$ $a_1 = -0.00164$	$n = 14$ $\nu = 12$ $RSS = 0.07325$ $t_{95} = 2.179$ $s_{TT} = 1.46E6$ $\bar{T} = 1396$	*[30]*	*Correlation valid between 800-1900K.*
iC_4H_8	*8,4*	$= a_0 + a_1 T$ $a_0 = 3.93$ $a_1 = -0.00106$	$n = 7$ $\nu = 5$ $RSS = 0.06012$ $t_{95} = 2.571$ $s_{TT} = 3.40E5$ $\bar{T} = 1189$	*[30]*	*Measured to be approximately the same as (10,4). Correlation fit to the combined data of (8,4) and (10,4). Correlation valid between 800-1900K.*
$1C_4H_8$	*8,5*	$= a_0 + a_1 T$ $a_0 = 4.37$ $a_1 = -0.001$	$n = 5$ $\nu = 3$ $RSS = 0.00505$ $t_{95} = 3.182$ $s_{TT} = 2.14E5$ $\bar{T} = 1345$	*[30]*	*Measured to be approximately the same as (10,5). Correlation fit to the combined data of (8,5) and (10,5). Correlation valid between 800-1900K.*
C_6H_6	*8,6*	*Approximately zero*		*[6]*	*Approximately zero*
C_7H_8	*8,7*	*Approximately zero*		*[6]*	*Approximately zero*
A1	*8,8*	*Unknown*			*Unknown*
A2	*8,9*	*Unknown*			*Unknown*
A3	*8,10*	*Unknown*			*Unknown*
C1	*8,11*	*Unknown*			*Unknown*
Cross-sections at 10.958 μm					
CH_4	*9,1*	*Approximately Zero*		*[6]*	*Approximately zero*
C_2H_4	*9,2*	$= a_0 + a_1 T$ $a_0 = 0.824$ $a_1 = (8.10)E - 4$	$n = 16$ $\nu = 14$ $RSS = 0.1939$ $t_{95} = 2.145$ $s_{TT} = 1.45E6$ $\bar{T} = 1020$	*[31,34] & new*	*Correlation valid between 600-1600K.*
C_3H_6	*9,3*	$= a_0 + a_1 \exp\left(-\frac{T - x_0}{b_1}\right) + a_2 \exp\left(-\frac{T - x_0}{b_2}\right)$ $a_0 = 2.7081$ $a_1 = 3.48$ $a_2 = 7.29$ $b_1 = 105.65$ $b_2 = 315.94$ $x_0 = 642.98$	$n = 36$ $\nu = 30$ $RSS = 1.746$ $t_{95} = 2.042$ $s_{TT} = 3.59E6$ $\bar{T} = 1037$	*[31,34] & new*	*Parise et al. [31] provide the following relation in units of [m^2/mol]:* $\left[\frac{m^2}{mol}\right] = 3.105 + 197.10 \exp\left(-\frac{\mathrm{T}}{216.47}\right)$ *Correlation valid between 600-1800K.*
iC_4H_8	*9,4*	$= a_0 + a_1 \exp\left(-\frac{T - x_0}{b_1}\right)$ $a_0 = 1.46$ $a_1 = 1.44$ $x_0 = 683.2$ $b_1 = 558.3$	$n = 8$ $\nu = 4$ $RSS = 0.01207$ $t_{95} = 2.776$ $s_{TT} = 6.5E5$ $\bar{T} = 984.58$	*new*	*Correlation valid between 600-1500K.*
$1C_4H_8$	*9,5*	$= a_0 + a_1 T + a_2 T^2 + a_3 T^3$ $a_0 = 8.87$ $a_1 = -0.00375$ $a_2 = -5.82E - 6$ $a_3 = 4.03E - 9$	$n = 18$ $\nu = 14$ $RSS = 0.964$ $t_{95} = 2.145$ $s_{TT} = 2.11E6$ $\bar{T} = 773.6$	*[34] & new*	*Correlation valid between 300-1500K.*
C_6H_6	*9,6*	*Approximately Zero*		*[6]*	*Approximately zero*
C_7H_8	*9,7*	$= a_0 + a_1 T$ $a_0 = 0.154$ $a_1 = 1.30E - 4$	$n = 4$ $\nu = 2$ $RSS = 7.492E - 4$ $t_{95} = 4.303$ $s_{TT} = 3.29E5$ $\bar{T} = 997.7$	*new*	*Large uncertainty*

A1	*9,8*	$= a_0 + a_1 T$ $a_0 = -1.16307$ $a_1 = (0.00225)$	$n = 50$ $\nu = 48$ $RSS = 83.81$ $t_{95} = 2.021$ $s_{TT} = 3.19E6$ $\bar{T} = 991.5$	*new*	*Large uncertainty. Correlation valid between 300-1400K.*
A2	*9,9*	$= a_0 + a_1 T$ $a_0 = -4.34937$ $a_1 = (0.00405)$	$n = 11$ $\nu = 9$ $RSS = 13.08$ $t_{95} = 2.262$ $s_{TT} = 7.60E5$ $\bar{T} = 1077$	*new*	*Large uncertainty. Correlation valid between 300-1400K.*
A3	*9,10*	$= a_0 + a_1 T$ $a_0 = 0.735$ $a_1 = (4.306)E - 4$	$n = 36$ $\nu = 34$ $RSS = 27.124$ $t_{95} = 2.042$ $s_{TT} = 2.41E6$ $\bar{T} = 1016$	*new*	*Large uncertainty. Correlation valid between 300-1400K.*
C1	*9,11*	$= a_0 + a_1 T$ $a_0 = 0$ $a_1 = 0.00115$	$n = 11$ $\nu = 10$ $RSS = 23.99382$ $t_{95} = 2.228$ $s_{TT} = 1.54E6$ $\bar{T} = 1066$	*new*	*Large uncertainty. Correlation valid between 300-1400K. Y-intercept was fixed by the author.*
Cross-sections at 10.962 µm					
CH_4	*10,1*	*Approximately zero*		*[6]*	*Approximately zero*
C_2H_4	*10,2*	$= a_0 + a_1 T$ $a_0 = 2.238$ $a_1 = (-3.33)E - 5$	$n = 7$ $\nu = 5$ $RSS = 0.01691$ $t_{95} = 2.571$ $s_{TT} = 9.87E5$ $\bar{T} = 1417$	*new*	*Measured to be approximately the same as (8,2). Correlation fit to the combined data of (8,2) and (10,2). Correlation valid between 900-1900K.*
C_3H_6	*10,3*	$= a_0 + a_1 \exp\left(-\frac{T - x_0}{b_1}\right)$ $a_0 = 0.815$ $a_1 = 4.24$ $x_0 = 1022.04$ $b_1 = 914.33$	$n = 14$ $\nu = 10$ $RSS = 0.246$ $t_{95} = 2.228$ $s_{TT} = 1.55E6$ $\bar{T} = 1357$	*[23]*	*Valid for 800-2000K. Correlation valid between 800-1900K.*
iC_4H_8	*10,4*	$= a_0 + a_1 T$ $a_0 = 3.93$ $a_1 = -0.00106$	$n = 7$ $\nu = 5$ $RSS = 0.06012$ $t_{95} = 2.571$ $s_{TT} = 3.40E5$ $\bar{T} = 1189$	*[23]*	*Measured to be approximately the same as (8,4). Correlation fit to the combined data of (8,4) and (10,4). Correlation valid between 800-1600K.*
$1C_4H_8$	*10,5*	$= a_0 + a_1 T$ $a_0 = 34.37$ $a_1 = -0.001$	$n = 5$ $\nu = 3$ $RSS = 0.00505$ $t_{95} = 3.182$ $s_{TT} = 2.14E5$ $\bar{T} = 1345$	*[23]*	*Measured to be approximately the same as (8,5). Correlation fit to the combined data of (8,5) and (10,5). Correlation valid between 800-1700K.*
C_6H_6	*10,6*	*Approximately zero*		*[6]*	*Approximately zero*
C_7H_8	*10,7*	*Approximately zero*		*[6]*	*Approximately zero*
A1	*10,8*	*Unknown*			*Unknown*
A2	*10,9*	*Unknown*			*Unknown*
A3	*10,10*	*Unknown*			*Unknown*
C1	*10,11*	*Unknown*			*Unknown*
Cross-sections at 11.345 µm					
CH_4	*11,1*	*Approximately zero*		*[6]*	*Approximately zero*

C_2H_4	*11,2*	$= a_0 + a_1 T$ $a_0 = 2.76$ $a_1 = (-5.05) * 10^{-4}$	$n = 12$ $\nu = 10$ $RSS = 0.0633$ $t_{95} = 2.228$ $s_{TT} = 7.77E5$ $\bar{T} = 1029$	*[34] & new*	*Correlation valid between 700-1400K.*
C_3H_6	*11,3*	$= a_0 + a_1 T$ $a_0 = 1.88$ $a_1 = (-6.67) * 10^{-5}$	$n = 16$ $\nu = 14$ $RSS = 0.4072$ $t_{95} = 2.145$ $s_{TT} = 1.00E6$ $\bar{T} = 1015$	*[34] & new*	*Correlation valid between 600-1500K.*
iC_4H_8	*11,4*	$= a_0 + a_1 T$ $a_0 = 9.39$ $a_1 = (-0.0036)$	$n = 23$ $\nu = 21$ $RSS = 3.94$ $t_{95} = 2.080$ $s_{TT} = 1.81E6$ $\bar{T} = 1122$	*[19] & new*	*Spearrin et al. [19] provide:* $[m2/mol]$ $= (16.91)\exp(-(0.00124)T)$ $+ 1.02$ *Correlation valid between 600-1700K.*
$1C_4H_8$	*11,5*	$= a_0 + a_1 T + a_2 T^2 + a_3 T^3 + a_4 T^4$ $a_0 = -3.82$ $a_1 = 0.0316$ $a_2 = -5.72E-5$ $a_3 = 4.31E-8$ $a_4 = -1.17E-11$	$n = 20$ $\nu = 15$ $RSS = 0.1024$ $t_{95} = 2.131$ $s_{TT} = 4.14E6$ $\bar{T} = 810.0$	*[34] & new*	*Small data and complex fit. However, forth order polynomial captures low and high temperatures within the scatter. Correlation valid between 300-1400K.*
C_6H_6	*11,6*	*Approximately Zero*		*[6]*	*Approximately zero*
C_7H_8	*11,7*	*Unknown*			*Unknown*
A1	*11,8*	$= a_0 + a_1 T$ $a_0 = -3.9475$ $a_1 = 0.00478$	$n = 14$ $\nu = 12$ $RSS = 22.81$ $t_{95} = 2.179$ $s_{TT} = 9.04E5$ $\bar{T} = 1001$	*new*	*Large uncertainty. Correlation valid between 300-1400K.*
A2	*11,9*	$= a_0 + a_1 T$ $a_0 = 1.142$ $a_1 = (5.16423)E-4$	$n = 22$ $\nu = 20$ $RSS = 11.1626$ $t_{95} = 2.086$ $s_{TT} = 1.38E6$ $\bar{T} = 998$	*new*	*Large uncertainty. Correlation valid between 300-1400K.*
A3	*11,10*	$= a_0 + a_1 T$ $a_0 = 0$ $a_1 = 5.25E-4$	$n = 30$ $\nu = 29$ $RSS = 7.79$ $t_{95} = 2.045$ $s_{TT} = 9.55E5$ $\bar{T} = 992.8$	*new*	*Large uncertainty. y-intercept fixed by the author. Correlation valid between 700-1400K.*
C1	*11,11*	$= a_0 + a_1 T$ $a_0 = 0$ $a_1 = 0.00204$	$n = 8$ $\nu = 7$ $RSS = 27.86$ $t_{95} = 2.365$ $s_{TT} = 4.78E5$ $\bar{T} = 983.64$	*new*	*Large uncertainty. y-intercept fixed by the author. Correlation valid between 700-1400K.*

6. Absorption cross-section data and correlations

6.1. Pressure- and temperature-dependent cross-sections

For three cases in Table 2, methane cross-sections demonstrate a strong pressure dependence. Figures 5-7(a) present absorption cross-section data in three-dimensional space (temperature, pressure, and cross-section), along with the provided fit, for methane at 3.1758 µm, 3.17595 µm, and 3.392 µm. Figures 5-7(b) provide an easy-to-reference two-dimensional representations of the pressure-dependent methane cross-section measurements. For low-pressure cases, shown as black squares in Fig. 5, the data exhibits a high sensitivity to pressure, which manifests itself as scatter in two-dimensional space.

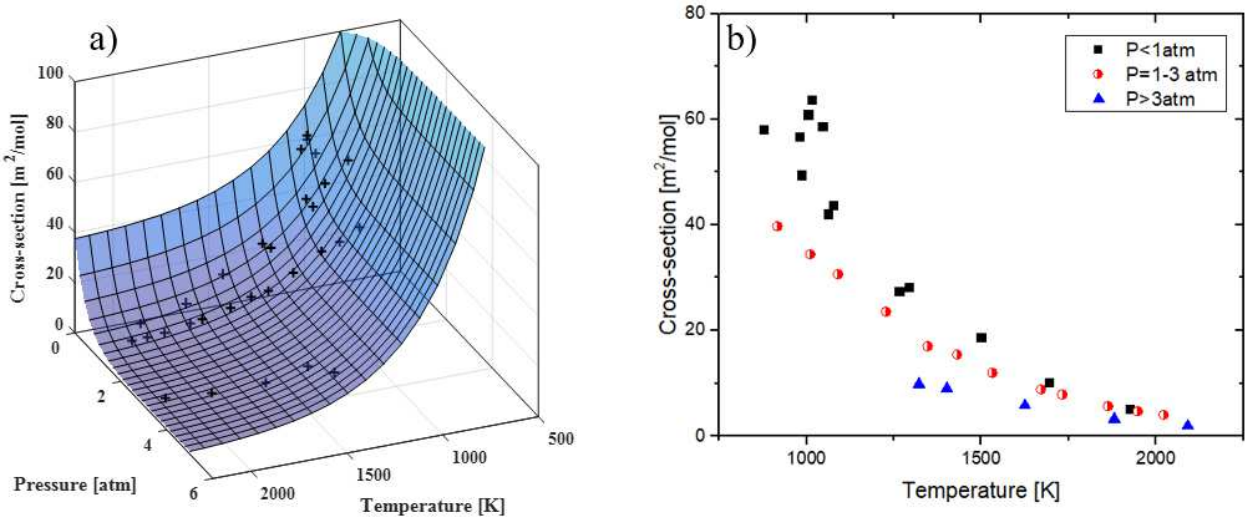

Fig. 5: CH_4 at 3.1758 µm. (a) the cross-section measurements of methane at 3.1758µm as a function of temperature and pressure and shown with the provided bivariate correlation. (b) A two-dimensional representation of the pressure dependence of methane at 3.1758 µm.

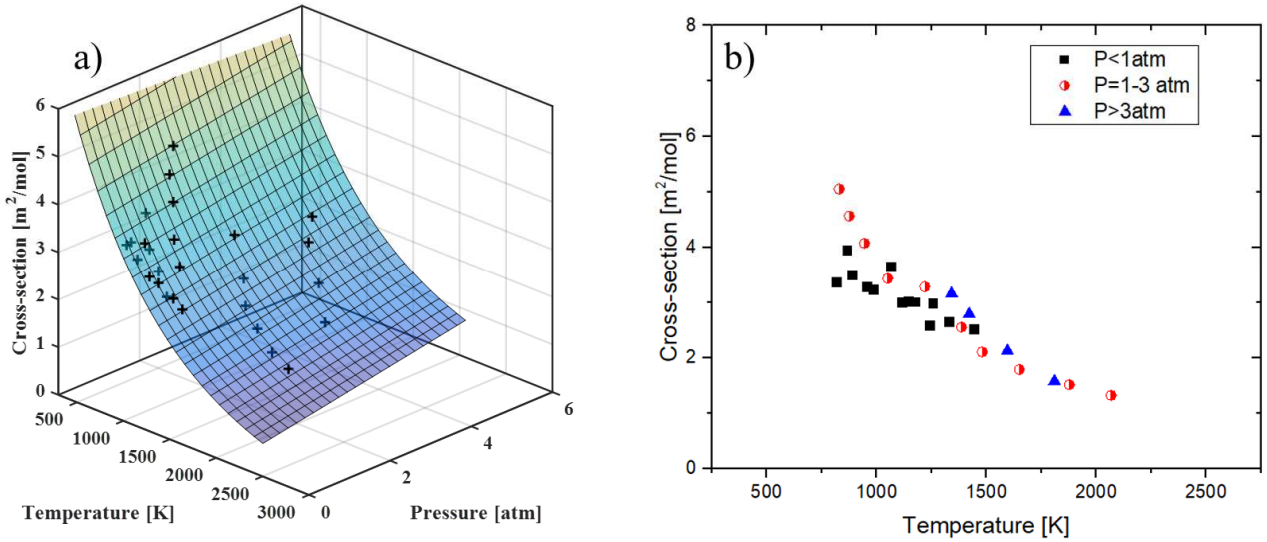

Fig. 6: CH_4 at 3.17595 µm. (a) The cross-section measurements of methane at 3.1758µm as a function of temperature and pressure and shown with the provided bivariate correlation. (b) A two-dimensional representation of the pressure dependence of methane at 3.17595 µm.

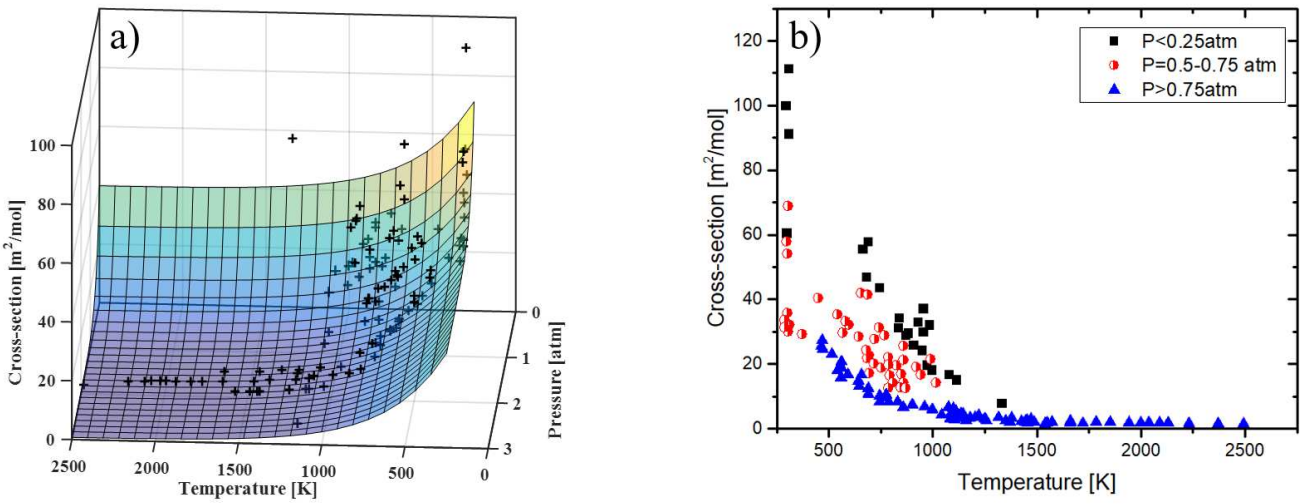

Fig. 7: CH_4 at 3.392 µm. (a) The cross-section measurements of methane at 3.392µm as a function of temperature and pressure and shown with the provided bivariate correlation. (b) A two-dimensional representation of the pressure dependence of methane at 3.392 µm.

6.2. High-temperature absorption cross-sections in the 3-4μm region

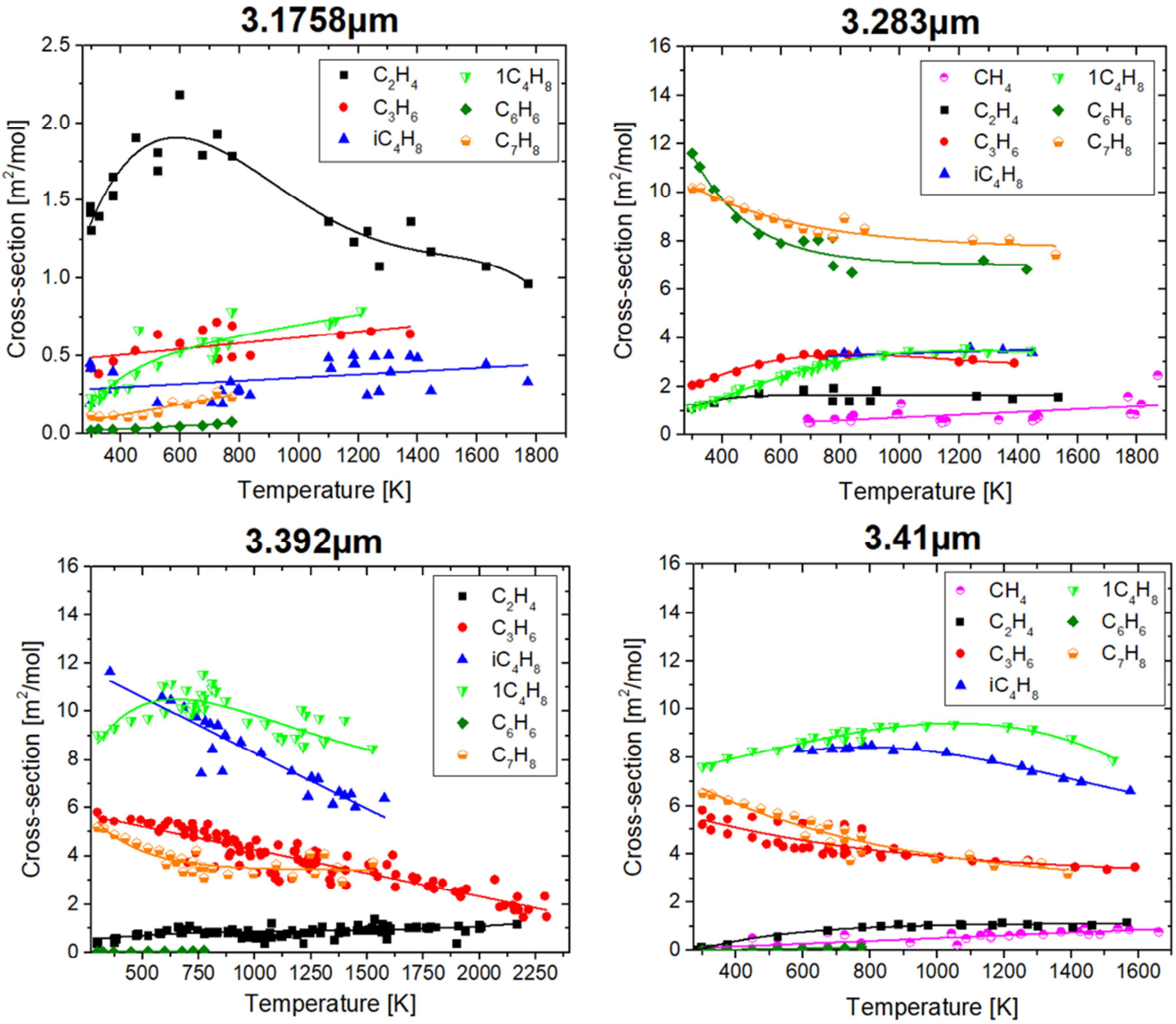

Fig. 8: Absorption cross-sections in the 3-4 μm region and the provided temperature-dependent correlations.

6.3 High-temperature absorption cross-sections in the 10-12μm region

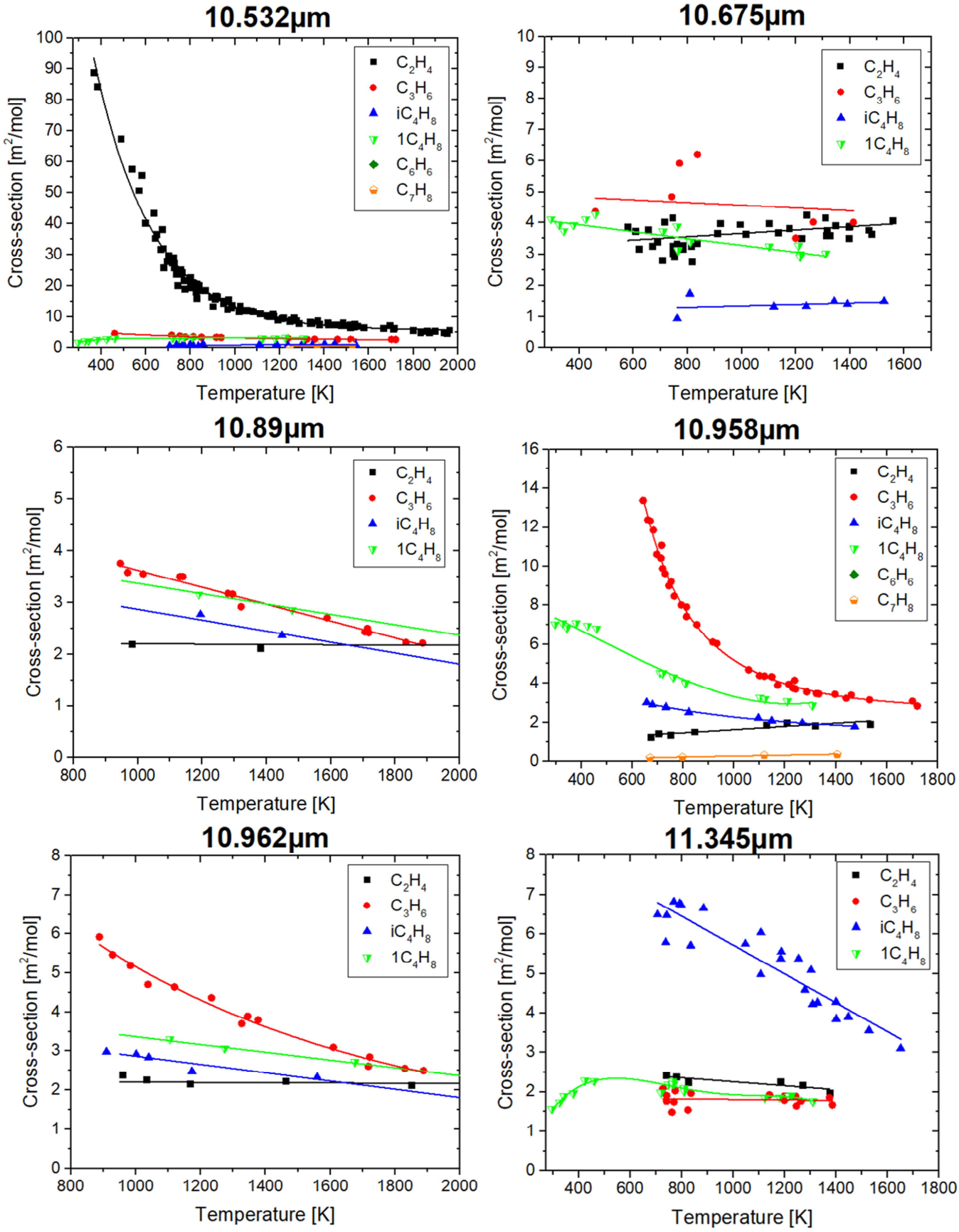

Fig. 9: Absorption cross-sections in the 10-12μm region and the provided temperature-dependent correlations.

7. Conclusions

There is growing motivation for high-temperature multi-species time-history measurements for reactive systems of gaseous molecules. Laser absorption spectroscopy offers a promising *in situ* and non-invasive method to provide these measurements by taking advantage of dissimilar mid-infrared spectra to identify different species. Historically, there has been a limited capability to measure enough of a mixture's spectrum at the short timescales required for speciation measurements of more than three species. This limited capability is partly due to the challenges associated with measuring spectra at temperatures where species are not thermally stable. Although novel lasers such as frequency comb EC-QCLs and rapidly tunable EC-QCLs may one day enable high-bandwidth measurement of broad spectral regions, this technology is still young [34-35]. While measurements of continuous spectra at high-temperature are not yet available, the measurement of spectra at discrete wavelengths has been the focus of much research dating back to the 1970s. Over the decades, many different wavelengths have been used for high-temperature laser absorption studies. To date, this spectral information has not been organized in a central location, which has impeded its usage.

In the present study, a framework for multi-wavelength speciation during hydrocarbon pyrolysis is presented. The proposed framework includes a suggested mathematical method for multi-wavelength measurements that takes advantage of recent advancements in convex optimization platforms. Additionally, a review is provided of pertinent fixed-wavelength mid-infrared laser absorption diagnostics that complement the proposed speciation method. In the review process, the authors suggest the use of a new laser diagnostic, at 3.283 µm, to measure the species time-histories of benzene and toluene during hydrocarbon pyrolysis. Lastly, a database of high-temperature absorption cross-sections is provided to enable the employment of the proposed framework. The database contains cross-sections for CH_4, C_2H_4, C_3H_6, i-C_4H_8, 1-C_4H_8, C_6H_6, C_7H_8 and samples of four jet fuel blends for the wavelengths of 3.1758 µm, 3.17595 µm, 3.283 µm, 3.392 µm, 3.41 µm, 10.532 µm, 10.675 µm, 10.89 µm, 10.958 µm, and 11.345 µm for temperatures and pressures within the range of 300-1600K and 0.25-4 atm. Measurements are provided from hundreds of new shock tube experiments alongside an aggregated dataset from literature. Care should be taken when using the provided correlations for temperatures beyond where the current data was fitted. Equipped with the current framework, a subsequent study will provide a demonstration pertaining to the pyrolysis of a simple hydrocarbon, and later for jet fuel pyrolysis.

Acknowledgements

This work was funded by the US Federal Aviation Administration (FAA) Office of Environment and Energy as a part of ASCENT Project 25 under FAA Award Number: 13-C-AJFE-SU-016. Any opinions, findings, and conclusions or recommendations expressed in this material are those of the authors and do not necessarily reflect the views of the FAA or other ASCENT sponsors. Author N. H. Pinkowski acknowledges financial support from the Department of Defense through the National Defense Science and Engineering Graduate (NDSEG) Fellowship.

References:

[1] M. B. Colket, J. S. Heyne, M. Rumizen, J. T. Edwards, M. Gupta, W. M. Roquemore, J. P. Moder, J. M. Tishkoff, C. Li, "An overview of the national jet fuels combustion Program," *54th AIAA Aerospace Sciences Meeting*. 2016.

[2] J. S. Heyne, M. B. Colket, M. Gupta, A. Jardines, J. P. Moder, J. T. Edwards, C. Li, M. Rumizen, "Year 2 of the national jet fuels combustion program: moving towards a streamlined alternative jet fuels qualification and certification Process" *55th AIAA Aerospace Sciences Meeting*. 2017.

[3] Y. Zhu, S. Wang, D.F. Davidson and R.K. Hanson, "Shock tube measurements of species time histories during jet fuel pyrolysis and oxidation," *53rd AIAA Aerospace Sciences Meeting*, 2015.

[4] D.F. Davidson, A. Tulgestke, Y. Zhu and R.K. Hanson. "Species time-history measurements during jet fuel pyrolysis and oxidation," *30th International Symposium on Shock Waves*, pp 309-312, 2017

[5] J.K. Shao, D.F. Davidson and R.K. Hanson, "Shock tube study of jet fuel pyrolysis and ignition at elevated pressure" *10th U.S. National Combustion Meeting*. 2017.

[6] S. Sharpe, T. Johnson, R. Sams, P. Chu, G. Rhoderick, P. Johnson, "Gas-Phase Databases for Quantitative Infrared Spectroscopy," *Society for Applied Spectroscopy*, vol. 58, No. 12, pp. 1452-1461, 2004.

[7] N. Jacquinet-Husson, R. Armante, N.A. Scott, A. Chedin, L. Crépeau, C. Boutammine, A. Bouhdaoui, C. Crevoisier, V. Capelle, C. Boonne, N. Poulet-Crovisier, A. Barbe, D. Chris Benner, V. Boudon, L.R. Brown, J. Buldyreva, A. Campargue, L.H. Coudert, V.M. Devi, M.J. Down, B.J. Drouin, A. Fayt, C. Fitteschen, J.M. Flaud, R.R. Gamache, J.J. Harrison, C. Hill, Ø Hodnebrog, S,M Hu, D. Jacquemart, A. Jolly, E. Jiménez, N.N. Lavrentieva, A.W. Liu, L. Lodi, O.M. Lyulin, S.T. Massie, S. Mikhailenko, H.S.P. Müller, O.V. Naumenko, A. Mikitin, C.J. Nielsen, J. Orphal, V.I. Perevalov, A. Perrin, E. Polovtseva, A. Predoi-Cross, M. Rotger, A.A. Ruth, S.S. Yu, K. Sung, S.A. Tashkun, J. Tennyson, VI.G. Tyuterev, J. Vander Auwera, B.A. Voronin, A. Makie, "The 2015 edition of the GEISA spectroscopic database", *Journal of Molecular Spectroscopy*, vol. 327, pp. 31-72, 2016.

[8] S.E. Stein, "Infrared spectra" in NIST Chemistry WebBook, NIST Standard Reference Database Number 69, Eds. P.J. Linstrom and W.G. Mallard, National Institute of Standards and Technology, Gaithersburg MD, 20899, https://doi.org/10.18434/T4D303, (retrieved November 14, 2018).

[9] L.S. Rothman, D. Jacquemart, A. Barbe, D. Chris Benner, M. Birk, L.R. Brown, M.R. Carleer, C. Chackerian Jr., K. Chance, L.H. Coudert, V. Dana, V.M. Devi, J.M. Flaud, R.R. Gamache, A. Goldman, Hartman J.M., Jucks K.W., Maki A.G., Mandin J.Y., Massie S.T., Orphal J., Perrin A., Rinsland C.P., Smith M.A.H., Tennyson J., Tolchenov R.N., Toth R.A., Vander Awera J., Varanasi P., and Wagner G, "The hitran 2004 molecular spectroscopic database," *Journal of Quantitative Spectroscopy and Radiative* Transfer, vol. 96, pp. 139-204, 2005.

[10] S. Li, Y. Zhu, D.F. Davidson and R.K. Hanson, "Pyrolysis study of conventional and alternative fuels behind reflected shock waves," *Fuel*, vol. 132, pp. 170-177, 2014.

[11] T. Parise, D.F. Davidson and R.K. Hanson, "Shock tube/laser absorption measurements of the pyrolysis of a bimodal test fuel," *Proceedings of the Combustion Institute*, vol. 36, pp. 281-288, 2016.

[12] W. Kun, R. Xu, T. Parise, J. Shao, A. Movaghar, D.J. Lee, J.W. Park, Y. Gao, T. Lu, F.N. Egolfopoulos, D.F. Davidson, R.K. Hanson, C.T. Bowman, H. Wang, "A physics-based approach to modeling real-fuel combustion chemistry – IV. HyChem modeling of combustion kinetics of a bio-derived jet fuel and its blends with a conventional Jet A" *Combustion and Flame*, vol. 198, pp. 477-489, 2018.

[13] H. Wang, R. Xu, K. Wang, C. Bowman, R.K Hanson, D. Davidson, K. Brezinsky, F.N. Egolfopoulos. "A physics-based approach to modeling real-fuel combustion chemistry – I. Evidence from experiments and thermodynamic, chemical kinetic and statistical considerations" *Combustion and Flame*, vol. 193, pp. 502-519, 2018.

[14] R. Xu, K. Wang, S. Banerjee, J. Shao, T. Parise, Y. Zhu, S. Wang, A. Movaghar, D.J. Lee, R. Zhao, X. Han, Y. Gao, T. Lu, K. Brezinsky, F. N. Egolfopoulos, D.F. Davidson, R.K. Hanson, C.T. Bowman, H. Wang "A physics-based approach to modeling real-fuel combustion chemistry – II. Reaction kinetic models of jet and rocket fuels" *Combustion and Flame*, vol. 193, pp. 520-537, 2018.

[15] Y. Tao, R. Xu, K. Wang, J. Shao, S.E. Johnson, A. Movaghar, X. Han, J.W. Park, T. Lu, K. Brezinsky, F.N. Egolfopoulos, D.F. Davidson, R.K. Hanson, C. T. Bowman, H. Wang, "A physics-based approach to modeling real-fuel combustion chemistry – III. Reaction kinetic model of JP10" *Combustion and Flame*, vol. 198, pp. 466-476, 2018.

[16] G. L. Pilla, D. F. Davidson, R. K. Hanson. "Shock tube/laser absorption measurements of ethylene time-histories during ethylene and n-heptane pyrolysis" *Proceedings of the Combustion Institute*, vol. 33, issue 1, pp. 333-340, 2011.

[17] D.R. Haylett, R.D. Cook, D.F. Davidson, R.K. Hanson, "OH and C_2H_4 species time-histories during hexadecane and diesel ignition behind reflected shocks waves," *Proceedings of the Combustion Institute*, vol. 33, pp. 167-173, 2011

[18] W. Ren, D.F. Davidson and R.K. Hanson, "IR laser absorption diagnostic for C_2H_4 in shock tube kinetics studies," *International Journal of Chemical Kinetics*, pp. 423-432, 2012.

[19] R.M. Spearrin, S. Li, D.F. Davidson, J.B. Jeffries and R.K. Hanson, "High-temperature iso-butene diagnostic for shock tube kinetics using a pulsed quantum cascade laser near 11.3 μm," *Proceedings of the Combustion Institute*, vol. 35, issue 3, pp. 3645-3651, 2015.

[20] D.B. Olson, W.G. Mallard, and W.C. Gardiner, Jr., "High temperature absorption of the 3.39 μm he-ne laser line by small hydrocarbons," *Applied Spectroscopy*, vol. 32, issue 5, pp. 489-493, 1978.
[21] T. Tsuboi, N. Arimitsu, D. Ping, and J.M. Hartmann, "Temperature, density, and perturber dependences of absorption of the 3.39 µm he-he laser by methane," *Japanese Journal of Applied Physics*, vol. 29, pp. 2147-2151, 1990.
[22] T. Tsuboi, N. Arimitsu, D. Ping, and J.M. Hartmann, "Further study on temperature, density, and perturber dependences of absorption of 3.39µm He-Ne laser by methane," *Japanese Journal of Applied Physics,* vol. 33, part 1, No. 9A, pp. 5062-5063, 1994.
[23] Y. Hidaka, T. Higashihara, N. Ninomiya, H. Oshita, H. Kawano. "Thermal isomerization and decomposition of 2-butyne in shock waves," *Journal of Physical Chemistry*, vol. 97, pp. 10977-10983, 1993.
[24] T. Koike and W.C. Gardiner, Jr., "High-temperature absorption of the 3.39 µm he-ne laser line by acetylene, ethylene, and propylene," *Applied Spectroscopy*, vol. 34, issue 1, pp. 81- 84, 1980.
[25] T. Tsuboi, K. Inomata, Y. Tsunoda, A. Isobe, and K. Nagaya. "Light absorption by hydrocarbon molecules at 3.392 µm of he-ne laser," *Japanese Journal of Applied Physics*, vol. 24, No. 1, pp. 8-13, 1985.
[26] S. Wang, T. Parise, S.E. Johnson, D.F. Davidson and R.K. Hanson, "A new diagnostic for hydrocarbon fuels using 3.41-micron diode laser absorption," *Combustion and Flame*, vol. 35, issue 3, pp. 129-139, 2015.
[27] D. Nativel, B. Shu, J. Herzler, M. Fikri, C. Schulz, "Shock-tube study of methane pyrolysis in the context of energy-storage processes," *Proceedings of the Combustion Institute*, in press, 2018.
[28] R. Sur, S. Wang, K. Sun, D.F. Davidson, J.B. Jeffries and R.K. Hanson, "High sensitivity interference free diagnostic for measurement of methane in shock tubes," *Journal of Quantitative Spectroscopy and Radiative Transfer*, vol. 156, pp. 80-87, 2015.
[29] M. E. MacDonald, W. Ren, D.F. Davidson, R.K. Hanson, W. Pitz, M. Mehl and C.K. Westbrook, "Fuel and ethylene measurements during n-dodecane, methylcyclohexane and iso-cetane pyrolysis in shock tubes," *Fuel*, vol. 103, pp. 1060-1068, 2013.
[30] R. Chrystie, E.F. Nasir, A. Farooq, "Propene concentration sensing for combustion gases using quantum-cascade laser absorption near 11 µm," *Applied Physics B*, vol. 120, issue 2, pp. 317-327, 2015.
[31] T. Parise, D. Davidson, R. Hanson, "Development of a two-wavelength IR laser absorption diagnostic for propene and Ethylene," *Measurement Science and Technology*, vol. 29, 2018.
[32] T Shimanouchi, "Tables of molecular vibration frequencies. consolidated volume II". *Journal of Physical and Chemical Reference Data*, vol. 6, issue 3, pp. 993-1102, 1977.
[33] S. J. Cassady, W. Y. Peng, R. K. Hanson. "Temperature-dependent line parameter study of acetylene transitions near 3 µm" *Journal of Quantitative Spectroscopy and Radiative Transfer*, in press, 2018.
[34] C. Strand, Y. Ding, S. Johnson, R.K. Hanson, "Measurement of the mid-infrared absorption spectra of ethylene (C_2H_4) and other molecules at high temperatures and pressures," *Journal of Quantitative Spectroscopy and Radiative Transfer*, in press, 2018.
[35] J. Faist, G. Villares, G. Scalari, M. Rösch, C. Bonson, A. Hugi, M. Beck, "Quantum Cascade Laser Frequency Combs," *Nanophotonics*, vol. 5, issue 2, pp. 272-291, 2016.
[36] M. F. Campbell, D. R. Haylett, D. F. Davidson, and R. K. Hanson. "AEROFROSH: a shock condition calculator for multi-component-fuel aerosol-laden flows," *Shock Waves*, vol. 26, issue 4, pp. 429-447, 2016.
[37] B.M.Gauthier, D.F. Davidson, R.K. Hanson, "Shock tube determination of ignition delay times in full-blend and surrogate fuel mixtures" *Combustion and Flame*, vol. 139, issue 3, pp. 300-311, 2004.
[38] M. Grant, S. Boyd. "CVX: Matlab software for disciplined convex programming," version 2.0 beta. http://cvxr.com/cvx, 2013.
[39] M. Grant and S. Boyd. "Graph implementations for nonsmooth convex programs, Recent Advances in Learning and Control (a tribute to M. Vidyasagar)," V. Blondel, S. Boyd, and H. Kimura, editors, *Lecture Notes in Control and Information Sciences, Springer*, pp. 95-110, 2008.
[40] I. Stranic, D.F. Davidson, R.K. Hanson, "Shock tube measurements of the rate constant for the reaction cyclohexene →ethlyene +1,3-butadiene," *Chemical Physics Letters*, vol. 584, pp. 18-23, 2013
[41] I. Stranic, R.K. Hanson, "Laser absorption diagnostic for measuring acetylene concentrations in shock tubes," *Journal of Quantitative Spectroscopy and Radiative Transfer*, vol. 142, pp. 58-65, 2014.
[42] I. Stranic, S.H. Pyun, D.F. Davidson, R.K. Hanson, "Multi-species measurements in 1-butanol pyrolysis behind reflected shock waves," *Combustion and Flame*, vol. 159, pp. 3242-3250, 2012.
[43] A.E. Klingbeil, J.B. Jeffries, R.K. Hanson, "Temperature-dependent mid-IR absorption spectra of gaseous hydrocarbons" *Journal of Quantitative Spectroscopy and Radiative Transfer*, vol. 107, Issue 3, pp. 407–420, 2007.

[44] E. Es-sebbar, Y. Benilan, A. Farooq., "Temperature-dependent absorption cross-section measurements of 1-butene (1-C_4H_8)" *Journal of Quantitative Spectroscopy and Radiative Transfer*. vol. 115, pp. 1-12, 2013.
[45] E. Es-sebbar, M. Alrefae, A. Farooq, "Infrared cross-section and integrated band intensities of propylene: Temperature-dependent studies," *Journal of Quantitative Spectroscopy and Radiative Transfer*. vol. 133, pp. 559-569, 2014.
[46] M. Alrefae, E. Es-sebbar, A. Farooq, "Absorption cross-section measurements of methane, ethane, ethylene, and methanol at high temperatures," *Journal of Molecular Spectroscopy*, vol. 303, pp. 8-14, 2014.
[47] E. Es-sebbar, A. Jolly, Y. Benilan, A. Farooq, "Quantitative mid-infrared spectra of allene and propyne from room to high temperatures," *Journal of Molecular Spectroscopy*, vol. 305, pp. 10-16, 2014.
[48] K.O. Petrov, S. Waltman, U. Simon, R.F. Curl, F.K. Tittel, E.J. Dlugokencky, L. Hollberg, "Detection of methane in air using diode-laser pumped difference-frequency generation near 3.2 µm," *Applied Physics B*, Vol. 61, Issue 6, pp. 553-558, 1995.
[49] K.P. Petrov, S. Waltman, E.J. Dlugokencky, M. Arbore, M.M. Fejer, F.K. Tittel, L.W. Hollberg, "Precise measurement of methane in air using diode-pumped 3.4-µm difference-frequency generation in PPLN," *Applied Physics B*, vol. 64, Issue 5, pp. 567-572, 1997.
[50] D. Richter, D.G. Lancaster, R.F. Curl, W. Neu, F.K. Tittel, "Compact mid-infrared trace gas sensor based on difference-frequency generation of two diode lasers in periodically poled $LiNbO_3$," *Applied Physics B*, vol. 67, issue 3, pp. 347-350, 1998.
[51] L. Goldberg, J. Koplow, D.G. Lancaster, R.F .Curl, F.K. Tittel, "Mid-infrared difference-frequency generation source pumped by a 1.1-1.5- dual-wavelength fiber amplifier for trace-gas detection," Optics Letters, vol. 23, issue 19, pp. 1517-1519, 1998.
[52] K.P. Petrov, A.T. Ryan, T.L. Patterson, L. Huang, S.J. Field, D.J. Bamford, "Mid-infrared spectroscopic detection of trace gases using guide-wave difference-frequency generation," *Applied Physics B*, vol. 67, issue 3, pp. 357-361, 1998.
[53] K.P. Petrov, A.T. Ryan, T.L. Patterson, L. Huang, S.J. Field, D.J. Bamford, "Spectroscopic detection of methane by use of guide-wave diode-pumped difference-frequency generation," *Optics Letters*, vol. 23, issue 13, pp. 1052-1054, 1998.
[54] D. Lancaster, D. Richter, R. Curl, and F. Tittel, "Diode lasers, DFG and Molecules," in *Advanced Semiconductor Lasers and Their Applications*, L. Hollberg and R. Lang, eds., *OSA Trends in Optics and Photonics*, vol. 31, paper 43, 1999.
[55] U. Gustafsson,J. Sandsten, S. Svanberg, "Simultaneous detection of methane, oxygen and water vapour utilizing near-infrared diode lasers in conjunction with difference-frequency generation", *Applied Physics B*, vol. 71, issue 6, pp. 853-857, 2000.
[56] H.Y. Clark, L. Corner, W. Denzer, G. Hancock, A. Hutchinson, M. Islam, R. Peverall, G.A.A. Ritchie, "Difference frequency deneration in periodically poled lithium niobate and its use in the detection of atmospheric methane," *Chemical Physics Letters*, vol. 399, issue 1-3, pp. 102-108, 2004.
[57] S.H. Pyun, J. Cho, D.F. Davidson, R.K. Hanson, "Interference-free mid-IR laser absorption detection of methane," *Measurement Science and Technology*, vol. 22, pp. 109, 2011.
[58] R.R Patty, G. M., Russwurm, W.A. McCleanny, D.R. Morgan, "CO_2 laser absorption coefficients for determining ambient levels of O_3, NH_3, and C_2H_4," Applied Optics, vol. 13, no. 12, pp. 2850-2854, 1974.
[59] U. Persson, B. Mathinsson, J. Johansson, S.T. Eng, "Temperature and pressure dependence of NH_3 and C_2H_4 absorption cross sections at CO_2 laser wavelengths," Applied Optics, vol. 19, no. 11, pp. 1711-1715, 1980
[60] J.N. Olsen, "Laser-initiated channels for ion transport: CO_2 laser absorption and heating of H_3 and C_2H_4 gases," *Journal of Applied Physics*, vol. 52, no. 5, p. 3279-3285, 1981.
[61] K. Wang, S.M. Villano, A.M. Dean, "Experimental and kinetic modeling study of butene isomer pyrolysis: Part I. 1- and 2-butene," Combustion and Flame, vol. 173, pp. 347-369, 2016.
[62] Y. Zhang, J. Cai, L. Zhao, J. Yang, H. Jin, Z. Cheng, Y. Li, "An experimental and kinetic modeling study of three butene isomers pyrolysis at low pressure," Combustion and Flame, vol. 159, pp. 905-917, 2012.
[63] J.A. Manion, I.A. Awan, "Evaluated kinetics of terminal and non-terminal addition of hydrogen atoms to 1-alkenes: a shock tube study of H+1-butene," *Journal of Physical Chemistry A*, vol. 119, pp. 429-441, 2015.
[64] Y. Li, C.W. Zhou, K.P. Somers, K.Zhang, H. J. Curran, "The oxidation of 2-butene: a high pressure ignition delay, kinetic modeling study and reactivity comparison with isobutene and 1-butene," *Proceedings of the Combustion Institute*, vol. 36, pp. 403-411, 2017.
[65] J.M. Andrésen, J.J. Strohm, L. Sun, C. Song, "Relationship between the formation of aromatic compounds and solid deposition during thermal degradation of jet fuels in the pyrolytic regime," *Energy & Fuels*, vol. 15, pp. 714-723, 2001.
[66] M.J. DeWitt, E. Corporan, J. Graham, D. Minus, "Effects of aromatic type and concentration in Fischer-Tropsch fuel on emissions production and material compatibility," *Energy and Fuels*, vol. 22, pp. 2411-2418, 2008.
[67] Y. Zhu. "Shock tube studies of kinetics of conventional and alternative engine fuels". *Stanford University*, Dissertation, 2016.
[68] H. Coleman, G. Steele, "Experimentation, validation, and uncertainty analysis for engineers", *John Wiley & Sons Inc.*, 2009, print

Technical Report Documentation Page

1. Report No.	2. Government Accession No.	3. Recipient's Catalog No.
j.jqsrt.2018.12.038		

4. Title and Subtitle	5. Report Date
A multi-wavelength speciation framework for high-temperature hydrocarbon pyrolysis	December 2018
	6. Performing Organization Code

7. Author(s)	8. Performing Organization Report No.
Nicolas H. Pinkowski, Yiming Ding, Sarah E. Johnson, Yu Wang, Thomas C. Parise, David F. Davidson, Ronald K. Hanson	

9. Performing Organization Name and Address	10. Work Unit No. (TRAIS)
Center of Excellence for: Alternative Jet Fuels and Environment Stanford University Department of Mechanical Engineering Stanford CA 94305	11. Contract or Grant No. 13-C-AFJE-SU-015

12. Sponsoring Agency Name and Address	13. Type of Report and Period Covered
Federal Aviation Administration Office of Environment and Energy	Journal Article
	14. Sponsoring Agency Code

15. Supplementary Notes

16. Abstract

A framework for the study of high-temperature hydrocarbon pyrolysis is presented. The proposed frame- work details a multi-wavelength speciation method using convex optimization, a review of complementary fixed-wavelength laser diagnostics, and a database of high-temperature absorption cross-sections to enable use of the framework for 11 different species. The proposed speciation method involves a vectorized Beer-Lambert system solved under solution constraints using convex optimization. In support of the proposed method, a review of pertinent laser diagnostics and a database of high-temperature absorption cross-sections are also provided. The database includes measured absorption cross-sections of methane (CH 4), ethylene (C 2 H 4), propene (C 3 H 6), isobutene (i-C 4 H 8), 1-butene (1-C 4 H 8), benzene (C 6 H 6), toluene (C 7 H 8), and four jet fuels (samples of Jet A, JP5, JP8, and Gevo ATJ) at the wavelengths of 3.1758 μm, 3.17595 μm, 3.283 μm, 3.392 μm, 3.410 μm, 10.532 μm, 10.675 μm, 10.89 μm, 10.958 μm, 10.962 μm, and 11.345 μm within the range of 30 0–160 0 K and 0.25–4 atm. The database is comprised of over 10 0 0 high–temperature absorption cross-section measurements from new shock tube experiments, new Fourier transform infrared spectrometer (FTIR) experiments, and an aggregated dataset from the literature. The convex speciation method and cross-section database provided will facilitate laser absorption studies of hydrocarbon pyrolysis used in the development of chemical kinetic mechanisms.

17. Key Words	18. Distribution Statement
Cross-section, Mid-infrared, Absorption spectroscopy, Hydrocarbon pyrolysis, High-temperature, Shock tube, Methane, Ethylene, Propene, Butene, Toluene, Benzene, Jet fuel, Convex optimization, ASCENT	

19. Security Classif. (of this report)	20. Security Classif. (of this page)	21. No. of Pages	22. Price
Unclassified	Unclassified		